
DATA VALUE IN THE AGE OF SCALING: UNDERSTANDING LLM SCALING DYNAMICS UNDER REAL–SYNTHETIC DATA MIXTURES

A PREPRINT

Haohui Wang Virginia Tech haohuiw@vt.edu	Jingyuan Qi Virginia Tech	Jianpeng Chen Virginia Tech	Jun Wu Michigan State University
Lifu Huang University of California, Davis	Lecheng Zheng Virginia Tech	Kevin Choi Deloitte	Balaji Veeramani Deloitte
Edward Bowen Deloitte	Alison Hu Deloitte	Tyler Cody Virginia Tech	Dawei Zhou Virginia Tech

November 18, 2025

ABSTRACT

The rapid progress of large language models (LLMs) is fueled by the growing reliance on datasets that blend real and synthetic data. While synthetic data offers scalability and cost-efficiency, it often introduces systematic distributional discrepancies, particularly underrepresenting long-tail knowledge due to truncation effects from data generation mechanisms like top- p sampling, temperature scaling, and finite sampling. These discrepancies pose fundamental challenges in characterizing and evaluating the utility of mixed real-synthetic datasets. In this paper, we identify a three-phase scaling behavior characterized by two breakpoints that reflect transitions in model behavior across learning head and tail knowledge. We further derive an LLM generalization bound designed for real and synthetic mixtures, revealing several key factors that govern their generalization performance. Building on our theoretical findings, we propose an effective yet efficient data valuation method that scales to large-scale datasets. Comprehensive experiments across four tasks, including image classification, sentiment classification, instruction following, and complex reasoning, demonstrate that our method surpasses state-of-the-art baselines in data valuation with significantly low computational cost.

1 Introduction

Large language models (LLMs) have achieved remarkable advances, driving unprecedented transformations across various tasks, including language understanding [1], generation [2], instruction following [3], and reasoning [4]. Despite these achievements, their performance is largely driven by the scale and quality of training datasets [5, 6]. To mitigate the scarcity and high cost of high-quality real data, many modern training pipelines incorporate synthetically generated data, which can be scaled efficiently through data augmentation or controlled generation [7, 8]. While synthetic data plays a critical role in scaling data at reduced cost, it often introduces systematic distributional discrepancies, resulting in unintended negative impacts on model performance [9]. In particular, synthetic datasets inherently bias training towards frequently occurring knowledge while neglecting rare but significant knowledge [10]. Consequently, such discrepancies can degrade the overall generalization capabilities of LLMs on downstream tasks, leading to model collapse and failure to capture underrepresented knowledge [11].

One potential explanation for this challenge lies in the inherent long-tail distribution of knowledge present in real-world data. Empirical studies have shown that real-world knowledge typically follows a long-tail distribution, where a small amount of prevalent (“head”) knowledge appears frequently, while numerous rare (“tail”) knowledge occur infrequently but collectively represent a significant portion of essential knowledge [12], as shown by the orange curve in Figure 1. For

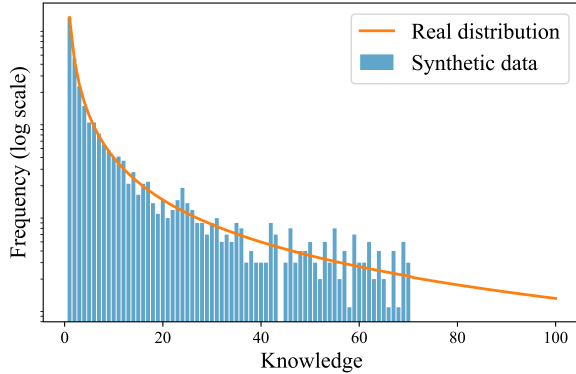


Figure 1: The real-world knowledge follows a long-tail distribution (illustrated with the greatest common divisor task [14]). Synthetic data is often sampled only from the head knowledge, leading to a truncated tail.

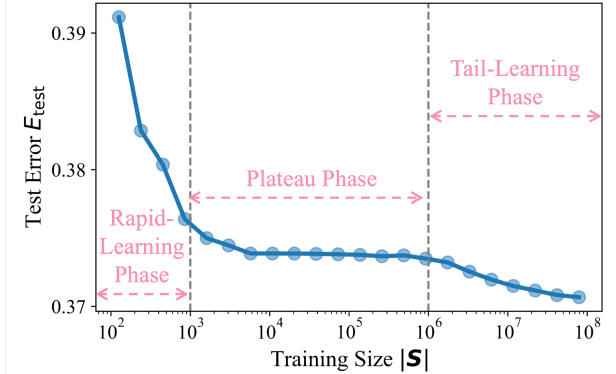


Figure 2: Fine-grained three-phase scaling behavior on real and synthetic mixtures, illustrated with the greatest common divisor task [14].

example, large language models usually perform well on general questions (e.g., normal disease diagnosis) but struggle when answering rare or highly specific questions (e.g., rare disease diagnosis) [13]. Synthetic data generation methods often exacerbate this imbalance in the distribution of knowledge because their inherent generation biases towards common knowledge make rare knowledge even more scarce in the training data. As a result, LLMs trained on datasets of real and synthetic mixtures exhibit complex scaling behaviors, reducing learning efficiency and generalization in pre-training and fine-tuning steps. These observations motivate us to ask two fundamental research questions: **(Q1)** What are the scaling behaviors of large language models when trained on real and synthetic mixtures, and how do these behaviors impact the acquisition of tail knowledge? and **(Q2)** How can we develop an salient data valuation framework to identify valuable subsets of data, thereby better guiding the training process under real and synthetic mixtures?

To address the first question **(Q1)** on the scaling behaviors of LLMs trained on real–synthetic data mixtures, we identify a *three-phase scaling pattern* in the training process of LLMs, as illustrated in Figure 2. In particular, an initial *Rapid-Learning Phase* dominated by frequent (“head”) knowledge present abundantly in both real and synthetic data; a subsequent *Plateau Phase*, in which additional data provides diminishing returns due to the limited coverage of rare (“tail”) knowledge in synthetic data; and a final *Tail-Learning Phase*, where sufficient real data containing the tail knowledge enables further performance gains. We further introduce a novel theoretical framework based on the LLM generalization bound. This framework reveals the generalization error in terms of empirical losses of real and synthetic mixtures, the distribution discrepancies between training and test distributions, the neural tangent kernel (NTK [15]) reflecting training dynamics, and the proportion of real data in the training set.

To empirically guide the LLM training process under real and synthetic mixtures and address the second research question **(Q2)**, we propose a scalable and theoretically grounded data valuation framework. Traditional data valuation techniques, such as Leave-One-Out (LOO [16]) and Shapley Values (SV [17]), require retraining the model multiple times on different subsets, which is computationally infeasible for models with millions of parameters [16, 18]. Our proposed data valuation framework is directly derived from our LLM generalization bound, enabling computationally efficient and theoretically grounded estimation of the contributions of individual data subsets without retraining, thereby potentially improving training efficiency to guide the training process under real and synthetic mixtures.

Finally, we empirically validate both our theoretical findings and the effectiveness of the proposed data valuation method through extensive experiments. Specifically, we evaluate our framework across four representative tasks, covering image classification, sentiment classification, instruction-following, and complex reasoning. Notably, we observe the predicted three-phase scaling behavior in an image classification task explicitly characterized by a known long-tail distribution. Furthermore, experimental results demonstrate that our valuation method outperforms existing baselines in effectively identifying high-value data subsets with a low computation cost. In particular, our valuation scores exhibit the highest correlation with ground-truth compared to the baseline methods, peaking at $\sim 20\times$ in the strongest case. We open-source our code at <https://github.com/wanghh7/3phaseLLM>.

2 Preliminary

In this section, we introduce the background that is pertinent to our work. Next, we briefly review notations, LLM scaling law, and LLM generalization.

Notations. Modern LLMs are increasingly trained on datasets composed of real and synthetic mixtures. Let $S = S_1 \cup S_2$ denote the training dataset, where $S_1 \sim \mathcal{D}$ consists of real data drawn from the true distribution \mathcal{D} , and $S_2 \sim \mathcal{D}'$ consists of synthetic data generated by model with an associated distribution \mathcal{D}' . We assume that the overall training

distribution can be written as:

$$\mathcal{D}_S = \pi \mathcal{D} + (1 - \pi) \mathcal{D}', \quad (1)$$

where $\pi \in [0, 1]$ is the proportion of real data in the training set. Suppose the total number of training samples is $|\mathcal{S}|$, then $\pi|\mathcal{S}|$ samples are drawn from \mathcal{D} and $(1 - \pi)|\mathcal{S}|$ from \mathcal{D}' . Model performance is evaluated on a test set \mathcal{T} of size $|\mathcal{T}|$, drawn from the distribution \mathcal{D}_T . Let $\mathcal{L}_S(f)$ denote the empirical error of model f on dataset \mathcal{S} , and $\mathcal{L}_{\mathcal{D}_T}(f)$ denote its generalization error on \mathcal{D}_T .

LLM Scaling Law. Scaling laws reveal how model performance improves with increasing dataset size, model parameters, and computational resources and guide large-scale training strategies [19, 6, 20]. In practical scenarios, a critical challenge arises from the reliance on synthetic data, which may lack the coverage of real-world data distribution. This reliance can lead to model collapse: as the model fits more synthetic samples, it reinforces biases from synthetic data \mathcal{D}' , exhibiting severe generalization degradation relative to the true distribution \mathcal{D} [11, 21, 22, 23]. Recent efforts attempt to extend scaling laws under real and surrogate data, but typically put strong modelling assumptions. For example, a common design draws independent samples from real and synthetic distributions that both belong to the Gaussian distribution $\mathbf{x} \sim \mathcal{N}(\mu, \Sigma)$, with different parameters. However, these efforts often overlook the long-tail nature of real-world knowledge.

LLM Generalization. To theoretically understand the LLM generalization, the neural tangent kernel has emerged as a powerful analytical framework for characterizing the training dynamics of neural networks with gradient descent [15]. Consider a L -layer LLM with m_l parameters in layer $l = 1, \dots, L$. Following prior literature [24], we assume $m_1 = \dots = m_{L-1} = m$ and $m_L = 1$ to simplify our analysis. Based on the formulation above, the NTK $\Theta \in \mathbb{R}^{|\mathcal{S}| \times |\mathcal{S}|}$ of a model $f(\mathbf{x}; \theta)$ on the dataset \mathcal{S} is defined as

$$\Theta(\mathbf{x}, \mathbf{x}'; \theta) = \nabla_{\theta} f(\mathbf{x}; \theta)^{\top} \nabla_{\theta} f(\mathbf{x}'; \theta), \quad (2)$$

where \mathbf{x} (or \mathbf{x}') denotes any data point in dataset \mathcal{S} . Interestingly, as $m_1, \dots, m_{L-1} \rightarrow \infty$, the NTK Θ_0 based on the initialized model parameters θ_0 will finally converge to a deterministic form Θ_{∞} [15, 25, 26]. However, existing LLM generalization bounds do not explicitly account for training on real and synthetic mixtures.

Problem Definition. The goal of this paper is to analyze LLMs under real and synthetic mixtures from two complementary perspectives. In particular, given the training set \mathcal{S} contain $\pi|\mathcal{S}|$ samples from true distribution \mathcal{D} and $(1 - \pi)|\mathcal{S}|$ from synthetic distribution \mathcal{D}' , how can we (1) theoretically reveal the scaling behavior of LLM model f as detailed in Section 3? and (2) how can we develop a data valuation framework that estimates the contribution of each data subset in \mathcal{S} to the model's performance as detailed in Section 4?

3 Theoretical Analysis

In this section, we first analyze a fine-grained three-phase transition in the scaling behavior of LLMs when trained on real and synthetic mixtures. We then derive a novel LLM generalization bound for real and synthetic mixtures, which reveals four key factors that govern the generalization performance.

Three Phase Transitions. To understand the scaling behaviors of LLMs when trained on real and synthetic mixtures and how these behaviors impact the acquisition of tail knowledge (**Q1**), we analyze the behavior of LLMs under a realistic training setup. While prior work has investigated scaling behaviors in the context of model collapse, these studies [27, 28, 21, 22] often rely on strong assumptions about model and data distributions (e.g., deterministic settings, simplified linear regression models, or infinite original samples). In contrast, we consider a practical scenario where the knowledge i in real data exhibits a long-tail distribution \mathcal{D} . In natural language datasets, the word or token frequencies often exhibit long-tail distributions (Zipf's law [29]), which means a few "head" tokens occur extremely frequently, while many "tail" tokens appear rarely. We therefore model the true distribution \mathcal{D} over knowledge i by:

$$p_i \propto i^{-\beta}, \quad i = 1, 2, \dots, \quad (3)$$

where $\beta > 1$ characterizes the tail heaviness. Furthermore, when generating synthetic data via LLMs, the resulting data distribution \mathcal{D}' typically exhibits truncation in the tail. Specifically, the techniques of synthetic data generation inherently truncate or narrow the original distribution of generated tokens, thereby cutting off or diminishing probabilities for less frequent (tail) tokens [22]. For example, top- p (nucleus) sampling, where tokens beyond a cumulative probability threshold are discarded; temperature scaling, which modifies the probability distribution sharpness; or finite-sample biases, which restrict observation of low-frequency tokens. We assume the synthetic data distribution p' mirrors the true distribution p up to a finite cutoff k : $p'_i \propto i^{-\beta}$ for $i \leq k$, and $p'_i = 0$ for $i > k$. Therefore, the training dataset of total size $|\mathcal{S}|$ is composed of real data p_i with proportion π and synthetic data p'_i with proportion $(1 - \pi)$, where data is drawn from the distribution \mathcal{D}_S with probability:

$$q_i = \pi p_i + (1 - \pi)p'_i. \quad (4)$$

We further assume that if knowledge i is observed in the training set, it is predicted correctly with probability $\rho(i) = ai^{-\alpha}, a > 0$; if knowledge i is not observed, the probability is $\gamma(i) = bi^{-\lambda}, b > 0$. Under the setting, we establish the following lemma for the test error on \mathcal{D}_T of this model with respect to the true data distribution \mathcal{D}_S : $\mathcal{L}_{\text{test}} = \mathbb{E}_{(\mathbf{x}, y) \sim \mathcal{D}_T} [\ell(f_{\mathcal{D}_S}(\mathbf{x}), y)]$, where $f_{\mathcal{D}_S}$ is the model on \mathcal{D}_S and ℓ is the loss function:

Lemma 1 (Scaling Behavior with Three phases). *Consider training data where the probability of knowledge i is $q_i = \pi p_i + (1 - \pi)p'_i$, where $p_i \propto i^{-\beta}$ and p'_i is cut off at rank k as defined above. The test error $\mathcal{L}_{\text{test}}$ exhibits distinct scaling regimes characterized by two breakpoints at sample sizes $|\mathcal{S}| = k^\beta$ and $|\mathcal{S}| = k^\beta/\pi$. We have¹:*

Phase 1 (Rapid-Learning): $|\mathcal{S}| \leq c_1 k^\beta$, where c_1 is absolute constant,

$$\mathcal{L}_{\text{test}} \asymp a |\mathcal{S}|^{\frac{1-\alpha-\beta}{\beta}} - b |\mathcal{S}|^{\frac{1-\lambda-\beta}{\beta}} + a k^{1-\alpha-\beta} - b k^{1-\lambda-\beta} + k^{1-\beta}. \quad (5)$$

Phase 2 (Plateau): $c_1 k^\beta < |\mathcal{S}| < c_2 k^\beta/\pi$, where c_2 is absolute constant, $\mathcal{L}_{\text{test}}$ enters a transition state as the limited presence of tail knowledge prevents the rapid learning.

Phase 3 (Tail-Learning): $|\mathcal{S}| \geq c_2 k^\beta/\pi$,

$$\mathcal{L}_{\text{test}} \asymp a(\pi |\mathcal{S}|)^{\frac{1-\alpha-\beta}{\beta}} - b(\pi |\mathcal{S}|)^{\frac{1-\lambda-\beta}{\beta}} + k^{1-\beta}. \quad (6)$$

Remark #1: For frequently occurring (head) knowledge indexed by 1 through k , the performance scaling exhibits a critical transition at sample size $|\mathcal{S}| = k^\beta$, corresponding to the first breakpoint in Figure 3.

Remark #2: For infrequently occurring (tail) knowledge beyond rank k , the performance scaling exhibits a critical transition at sample size $|\mathcal{S}| = k^\beta/\pi$, corresponding to the second breakpoint Figure 3.

Remark #3: This lemma highlights three phases of performance improvement as training size $|\mathcal{S}|$ grows. As shown in Figure 3, initially in the rapid-learning phase, rapid performance gains occur predominantly due to extensive coverage and repeated sampling of head knowledge, supported by both real and synthetic data. As head knowledge becomes saturated, a plateau phase follows, characterized by minimal improvements. This stagnation arises because the model gains limited additional information from redundant head knowledge, and the data distribution has not yet yielded sufficient tail-class observations. Leveraging targeted data valuation strategies (as introduced in Section 4), one can efficiently identify and prioritize underrepresented knowledge, potentially improving training efficiency. Finally, in the tail-learning phase, the model’s performance significantly improves again as it learns from substantial accumulated real samples of tail knowledge.

LLM Generalization Bound. To provide a general theoretical understanding of LLMs trained on real–synthetic data mixtures, we derive a novel generalization bound with relaxed assumptions. Existing generalization bounds typically assume that all training data are drawn i.i.d. from a single distribution [30]. However, this assumption is overly simplistic for practical scenarios, as real-world datasets often supplement limited real datasets with synthetic data generated from large models. Our LLM generalization bound reflects a realistic and growing training regime in LLMs. It explicitly quantifies how empirical losses on training data of real–synthetic mixtures, the distributional discrepancies, the NTK, and data composition collectively influence the expected test loss.

To characterize the distribution discrepancy under the setting of real and synthetic mixtures, we introduce the \mathcal{H} -discrepancy $d_{\mathcal{H}}$ (Definition 1) in Appendix A. To analyze the training dynamics of LLMs, we employ the NTK. Following the assumptions in Shu et al. [31], we assume that the existence of a function class \mathcal{H} such that for any \mathbf{x} , the deviation between the model $f(\mathbf{x}; \boldsymbol{\theta}) \in [0, 1]$ and the optimal hypothesis $f^*(\mathbf{x}; \boldsymbol{\theta}) = \arg \min_f (\mathcal{L}_{\mathcal{D}_T}(f) + \mathcal{L}_{\mathcal{D}_S}(f))$ is bounded by some $h \in \mathcal{H}$ with $h(\mathbf{x}) \leq 1$. Our generalization bound is then derived based on both the NTK at initialization $\boldsymbol{\Theta}_0$ and at convergence $\boldsymbol{\Theta}_\infty$, and the distribution discrepancy between \mathcal{S}_1 , \mathcal{S}_2 , and \mathbf{T} :

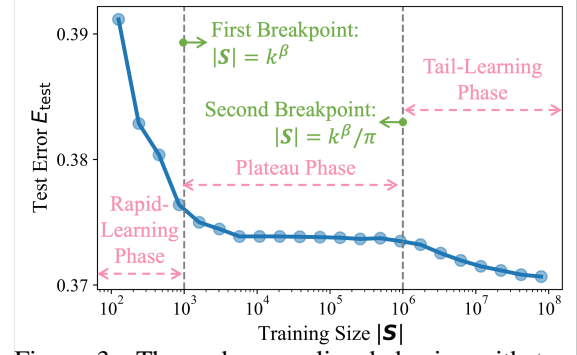


Figure 3: Three-phase scaling behavior with two breakpoints on real–synthetic mixtures, for the same task as Figure 2.

¹The notation $g(n) \asymp h(n)$ means that $c_1 h(n) \leq g(n) \leq c_2 h(n)$ for sufficiently large n and absolute constants $c_1, c_2 > 0$.

Theorem 1 (LLM Generalization Bound under Real and Synthetic Mixtures). *Let $\lambda_{\min}(\cdot)$ and $\lambda_{\max}(\cdot)$ denote the minimum and maximum eigenvalue of a matrix. Assume $\lambda_{\min}(\Theta_0) > 0$ and $\|\nabla_{\theta} f(\mathbf{x}; \theta_0)\|_2 \leq B$ for any $(\mathbf{x}, y) \in \mathcal{S}$ with $\|\mathbf{x}\|_2, y \in [0, 1]$. There exist $M \in \mathbb{N}$ such that for every $m > M$, when applying gradient descent with learning rate $\eta < \min \left\{ 2m^{-1} (\lambda_{\min}(\Theta_{\infty}) + \lambda_{\max}(\Theta_{\infty}))^{-1}, |\mathcal{S}|/\lambda_{\max}(\Theta_0) \right\}$, with probability at least $1 - 2\delta$,*

$$\begin{aligned} \mathcal{L}_{D_T}(f) &\leq \pi \mathcal{L}_{S_1}(f) + (1 - \pi) \mathcal{L}_{S_2}(f) + \pi d_{\mathcal{H}}(\mathbf{T}, \mathcal{S}_1) + (1 - \pi) d_{\mathcal{H}}(\mathbf{T}, \mathcal{S}_2) \\ &\quad + 2B \sqrt{\frac{\hat{\mathbf{y}}^T \Theta_0^{-1} \hat{\mathbf{y}}}{|\mathcal{S}|}} + \sqrt{\frac{2 \max(\pi, 1 - \pi) \log(8/\delta)}{|\mathcal{S}|}} + \varepsilon, \end{aligned} \quad (7)$$

where each element in $\hat{\mathbf{y}}$ is defined as $\hat{\mathbf{y}} \triangleq \mathbf{y} - f(\mathbf{x}; \theta_0)$ and $\varepsilon \triangleq 2c/\sqrt{m} + 3\sqrt{\log(4/\delta)/2|\mathcal{S}|} + \sqrt{\log(4/\delta)/2|\mathbf{T}|} + \mathcal{L}_{D_T}(f^*) + \mathcal{L}_{D_S}(f^*)$, and $c > 0$ is a constant.

Remark: Theorem 1 shows that the generalization error on the test distribution is bounded in terms of four key factors: (1) the empirical loss on training real samples and training synthetic samples; (2) the distribution discrepancy between test data and train data of real and synthetic mixtures; (3) the NTK-related value at initialization; and (4) the composition of the training dataset, specifically the proportion π of real data and the total number of samples $|\mathcal{S}|$.

4 Method

In this section, we introduce a data valuation framework designed for training settings involving real–synthetic data mixtures to solve **Q2**. Existing data valuation methods [32, 33, 34, 35, 36] typically require multiple retrainings or assume that all training data is drawn from a single distribution. These methods are not scalable to large models and, more importantly, do not explicitly consider the real-world data composed of real and synthetic mixtures. Our method is derived directly from the generalization bound in Section 3, and is designed to estimate the contribution of data subsets (data contributors) under real–synthetic mixtures, while remaining retraining-free and thus scalable to LLMs.

Specifically, we realize the discrepancy $d_{\mathcal{H}}$ using multiple-kernel maximum mean discrepancy (MK-MMD [37]) in reproducing kernel Hilbert spaces [38, 39], which captures a wide class of hypotheses while retaining computational efficiency. Moreover, the use of multiple kernels enables adaptive integration of features at different scales, which is well-suited for LLM training scenarios where real and synthetic data may differ significantly in linguistic style, topical coverage, or vocabulary distribution [40]. In data valuation, we compare the relative performances of data contributors; the constant ε in Theorem 1 is independent of the ranking of data contributors. We therefore ignore ε while reducing computational cost. Given a training dataset $\mathcal{S} = \mathcal{S}_1 \cup \mathcal{S}_2$, where $\mathcal{S}_1 \sim \mathcal{D}$ (real data) and $\mathcal{S}_2 \sim \mathcal{D}'$ (synthetic data), and a test distribution $\mathbf{T} \sim \mathcal{D}_T$, we define the data valuation score as (see Algorithm 1 in Appendix B):

$$\begin{aligned} v(\mathcal{S}) &= w_1 [\pi \mathcal{L}_{S_1}(f) + (1 - \pi) \mathcal{L}_{S_2}(f)] + w_2 [\pi \text{Dist}(\mathbf{T}, \mathcal{S}_1) + (1 - \pi) \text{Dist}(\mathbf{T}, \mathcal{S}_2)] \\ &\quad + w_3 \sqrt{\frac{\hat{\mathbf{y}}^T \Theta_0^{-1} \hat{\mathbf{y}}}{|\mathcal{S}|}} + w_4 \sqrt{\frac{\max(\pi, 1 - \pi)}{|\mathcal{S}|}}, \end{aligned} \quad (8)$$

where $\mathcal{L}_{S_i}(f)$ denotes the empirical loss on real ($i = 1$) or synthetic ($i = 2$) data, Dist is the MK-MMD metric [37], f and Θ_0 are the model and empirical NTK at initialization. $\hat{\mathbf{y}}$ is evaluated on dataset \mathcal{S} following its definition in Theorem 1. π is the proportion of real data in the training set, w_1, w_2, w_3, w_4 balance the contribution of the four terms.

The valuation function $v(\mathcal{S})$ in Eq.(8) directly reflects the components in our theoretical generalization bound. Each component of the empirical losses, distribution discrepancies, and the NTK, corresponds to a measurable quantity that influences generalization performance. This translation from theory to scoring function is particularly suited for LLMs, where large-scale training makes retraining-based valuation infeasible. The valuation function also provides a practical handle on the three-phase scaling behavior in Section 3. In the first phase, $v(\mathcal{S})$ highlights subsets from head classes that rapidly reduce the empirical losses. During the plateau phase, where head-class performance saturates, the NTK-based generalization term becomes critical, distinguishing data that meaningfully alters the function class from data that is redundant or uninformative. In the final phase, as tail classes begin to appear in real data, the function prioritizes examples that drive continued error reduction. Notably, our scoring function $v(\mathcal{S})$ is designed to be directly applicable in LLM-scale settings, but it also supports integration with marginal-contribution-based valuation methods, see Appendix C for details.

5 Experiments

In this section, we evaluate the effectiveness of our data valuation method under datasets of real and synthetic mixtures. We conduct experiments across four representative tasks: image classification, sentiment classification, instruction following, and complex reasoning. As detailed in Section 5.2, we first verify that the three-phase generalization behavior

predicted by our theoretical analysis emerges in practice under a controlled long-tail setting. Section 5.3 compares our method against five recent data valuation baselines across all tasks and various backbones. Our method achieves higher correlation with ground-truth while maintaining significantly low computational cost. Finally, Section 5.4 demonstrates that the relative values computed using our scoring function remain stable under subsampling, supporting the scalability of our framework for large-scale LLM tasks. Beyond the main results, we include an extended analysis of contributors’ ranking visualization across data valuation methods in Appendix E.

5.1 Experimental Setup

Tasks and Datasets. We consider the following four tasks: (1) *Image Classification* is the task of assigning a label to a given image. We use the CIFAR-100 dataset [41] as the real data, and generate synthetic data by applying corruption transformations from the CIFAR-100-C benchmark [42]. (2) *Sentiment Classification* is the task of determining the sentiment polarity (positive or negative) of a given text, such as a movie review. We use the IMDb [43] as the real dataset and the FinGPT Sentiment Train dataset [44] as synthetic data. (3) *Instruction Following* involves generating an appropriate response or action based on a natural language instruction, testing a model’s ability to comprehend and execute commands or answer questions accurately. We use the Natural-Instructions dataset [45] as the real dataset and the Magpie-Pro-1M dataset [46] as the synthetic dataset. (4) *Complex Reasoning*, particularly in mathematical problem-solving, requires generating multi-step reasoning processes to arrive at a solution, often using a technique called chain-of-thought (CoT) reasoning, where the model breaks down a problem into intermediate steps before providing the final answer. We use the human-annotated portions of the NuminaMath-CoT training set [47] as real data and the synthetically generated portions as synthetic data.

Baselines. We compare against five representative baselines designed for efficient data valuation: *DAVINZ* [48], *Deviation* [32], *LOGRA* [49], *TracIn* [50], and *TRAK* [51]. These baselines are selected based on two criteria: (1) they do not require repeated model retraining, making them scalable to LLMs; and (2) they operate with access to checkpoints, gradients, and training/test data.

Implementation Details. For all tasks, each method receives the same inputs: training data (real and synthetic), test data, model checkpoints, and access to model gradients. Due to the large-scale nature of LLM, we compute gradients for only 1% of the training data when evaluating gradient-based baselines to reduce computational overhead and improve efficiency. We use ResNet-18 for image classification task. For sentiment classification, instruction following, and complex reasoning tasks, we consider four backbones, including Qwen2.5-0.5B, Qwen3-0.6B, Qwen3-1.7B, and Llama-3.2-1B-Instruct. We use the Pearson, Spearman, and Kendall correlations between the data valuation scores and the ground truth as evaluation metrics. Following prior work [48], we use ground truth to refer to the test performance of models trained to convergence on different subsets of data. Specifically, the ground truth represents test accuracy for image classification and sentiment classification tasks, IFEval score for instruction following, and correctness for complex reasoning achieved by fully trained models, where each model is trained using data from different contributors. Further details about the experimental setups are provided in Appendix D.

5.2 Validating Theoretical Analysis

To empirically validate our theoretical insights on the three-phase scaling behavior in Section 3, we conduct experiments using CIFAR-100 as the real data and its corrupted variant (CIFAR-100-C) as the synthetic data. The proportion of real data is set to $\pi = 0.0625$, and we vary the total training sample size from 10^2 to 10^6 . We treat each of the 100 classes as one knowledge. To simulate a long-tail distribution, we manually construct a class frequency with $p_i \propto i^{-2}$ and apply a tail cutoff at $k = 70$. The model backbone is ResNet-18. We evaluate the test performance on a balanced test set with 10,000 samples, measuring both accuracy and loss separately for the overall classes, head classes ($i \leq 70$), and tail classes ($i > 70$). Figures 4 and 5 plot the model’s accuracy and test loss, respectively, as the increase of training sample size $|S|$. The results exhibit a three-phase behavior consistent with our theoretical predictions: Phase 1 (rapid-learning), we observe a sharp decrease in head-class loss, indicating that the model quickly learns head knowledge from both real and synthetic data. Phase 2 (plateau), the overall loss reduction slows down, reflecting diminishing returns from saturated head information. Phase 3 (tail-learning), tail-class accuracy improves and loss drops rapidly, as the model learns tail knowledge from the increased number of real data.

In addition, we further validate our theoretical results with respect to diverse mixture ratios π ranging from 0 to 1. The knowledge follows a long-tail distribution with $\beta = 1.5$ and tail cutoff $k = 100$. The model predicts a knowledge i correctly with probability $\rho(i) = i^{-0.5}$ if observed and $\gamma(i) = i^{-1}$ if unobserved. Figure 6 demonstrates that the three-phase scaling behavior holds consistently across different mixture ratios of real and synthetic data.

5.3 Effective and Efficient Data Valuation

We compare our method against five recent baselines across the four tasks, including image classification, sentiment classification, instruction following, and complex reasoning. Effectiveness is measured by correlations between data valuation scores and ground-truth including Pearson, Spearman, and Kendall correlations, and efficiency is assessed by runtime.

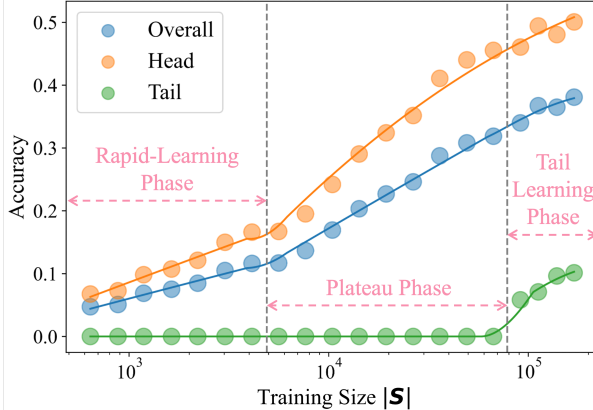


Figure 4: Model accuracy as the increase of training size $|S|$ on CIFAR-100, under a long-tail class distribution. Dashed grey lines mark predicted transition breakpoints at $|S| = k^\beta$ (left) and $|S| = k^\beta/\pi$ (right).

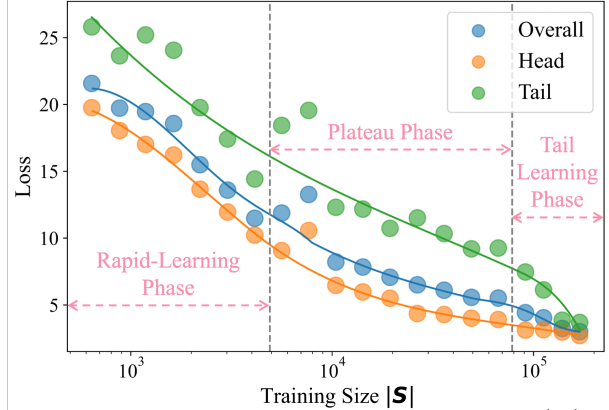


Figure 5: Test loss as the increase of training size $|S|$ on CIFAR-100, under a long-tail class distribution. Dashed grey lines mark predicted transition breakpoints at $|S| = k^\beta$ (left) and $|S| = k^\beta/\pi$ (right).

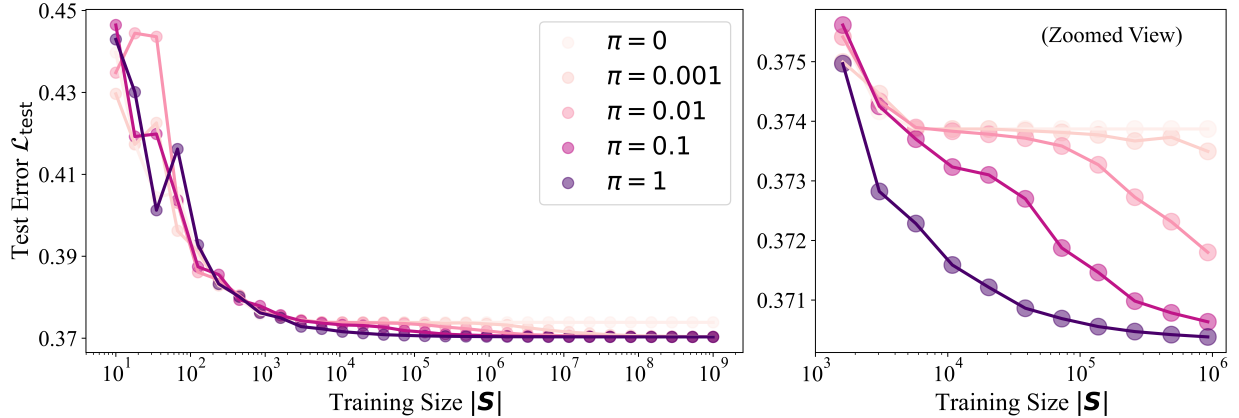


Figure 6: Simulation of three-phase scaling behavior under real-synthetic mixtures. Each curve represents a different mixture ratios of real and synthetic data π . The right panel shows a zoomed view of the range $|S| \in [10^3, 10^6]$.

From Figure 7, Figure 8, and Table 1, we have the following observations: (1) Across most tasks and backbones, our method achieves the highest correlation scores with ground-truth performance, and these gains are consistent across correlation measures, demonstrating its effectiveness in identifying valuable data contributors. In particular, on the sentiment task with Qwen3-1.7B, our approach attains a Spearman correlation of 0.81, significantly exceeding the second-best method of 0.32. (2) In addition to its effectiveness, our method incurs a low runtime, requiring only 8 seconds on average. This is significantly faster than Retrain (627 seconds), Deviation (553 seconds), and TRAK (166 seconds), highlighting better computational efficiency.

5.4 Stability of Relative Valuation Under Subsampling

To examine the stability of our method under subsampled training sets, we analyze whether MMD score $\pi \text{Dist}(\mathbf{T}, \mathbf{S}_1) + (1 - \pi) \text{Dist}(\mathbf{T}, \mathbf{S}_2)$ and NTK score $\sqrt{\hat{\mathbf{y}}^\top \Theta_0^{-1} \hat{\mathbf{y}}} / |\mathbf{S}|$ in Eq.(8) remain stable when computed on a small fraction of the data. Specifically, we conduct an image classification task with the first five contributors, and compute their scores using training subsets of size 100, 400, 1,000, and 4,000. For comparability, we apply min-max normalization to the scores within each subsampling size, focusing on the relative rankings rather than absolute values.

As shown in Table 2, both MMD and NTK scores maintain stability in their relative contributor rankings across different subsample sizes. For example, contributor 1 consistently receives the lowest normalized MMD and NTK scores, while contributor 5 consistently receives the highest score, regardless of training size. This suggests that the relative quality of contributors given by our method is consistent across diverse subsampling sizes.

6 Related Work

Data Valuation. Data valuation methods quantify the contribution or importance of individual data subsets of a dataset to the performance of machine learning models. Traditional retraining-based approaches, such as LOO [52, 16], SV-based methods [17], and downsampling [53], require extensive computation due to model retraining, making them

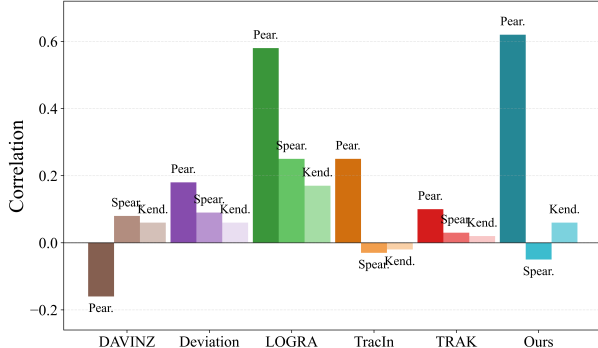


Figure 7: Comparison of data valuation methods on the image classification task. We report Pearson, Spearman, and Kendall correlations, with higher values indicating better performance.

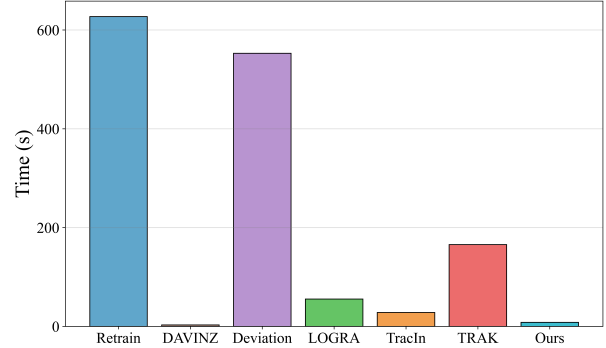


Figure 8: Runtime (in seconds) of data valuation methods on the image classification task. The reported values represent the average time for all data contributors.

Table 1: Comparison of data valuation methods across three tasks: sentiment classification, instruction following, and complex reasoning. For each task, we report the Pearson, Spearman, and Kendall correlations, where higher is better (\uparrow). The best results are shown in bold.

Backbone	Method	Sentiment			Instruction			Reasoning		
		Pear.	Spear.	Kend.	Pear.	Spear.	Kend.	Pear.	Spear.	Kend.
Qwen2.5-0.5B	DAVINZ	-0.46	-0.42	-0.33	-0.16	-0.40	-0.33	-0.00	-0.02	-0.01
	Deviation	0.63	0.76	0.56	0.05	-0.20	0.00	-0.03	0.00	-0.00
	LOGRA	-0.64	-0.79	-0.60	-0.09	0.20	0.00	0.08	0.08	0.05
	TracIn	-0.68	-0.81	-0.64	-0.94	-1.00	-1.00	-0.11	-0.12	-0.09
	TRAK	0.43	0.36	0.29	-0.01	0.20	0.00	-0.15	-0.14	-0.10
	Ours	0.70	0.87	0.64	1.00	1.00	1.00	0.11	0.14	0.10
Qwen3-0.6B	DAVINZ	-0.67	-0.71	-0.49	0.88	0.80	0.67	0.04	0.06	0.04
	Deviation	0.32	0.20	0.13	-0.80	-0.80	-0.67	0.14	0.15	0.10
	LOGRA	-0.62	-0.77	-0.58	-0.87	-0.80	-0.67	-0.07	-0.04	-0.03
	TracIn	-0.69	-0.66	-0.49	-0.87	-0.80	-0.67	0.05	0.06	0.04
	TRAK	0.64	0.73	0.54	-0.91	-0.80	-0.67	-0.01	-0.02	-0.02
	Ours	0.86	0.71	0.63	1.00	1.00	1.00	0.25	0.26	0.18
Qwen3-1.7B	DAVINZ	-0.41	-0.32	-0.33	0.66	0.20	0.00	0.43	0.41	0.30
	Deviation	-0.23	-0.52	-0.42	-0.87	-0.80	-0.67	-0.10	-0.09	-0.07
	LOGRA	0.19	0.24	0.11	-0.60	-0.20	0.00	-0.41	-0.40	-0.30
	TracIn	-0.03	0.02	0.07	-0.63	-0.60	-0.33	0.22	0.34	0.24
	TRAK	0.40	0.32	0.33	-0.60	-0.20	0.00	-0.17	-0.18	-0.13
	Ours	0.70	0.81	0.69	1.00	1.00	1.00	0.44	0.41	0.30
Llama-3.2-1B-Instruct	DAVINZ	0.70	0.62	0.45	0.14	0.80	0.67	-0.11	-0.06	-0.04
	Deviation	0.59	0.79	0.58	-0.05	-0.40	-0.33	0.16	0.15	0.10
	LOGRA	0.51	0.65	0.49	-0.07	-0.80	-0.67	-0.06	0.06	0.05
	TracIn	0.63	0.45	0.36	0.27	0.00	0.00	-0.04	-0.18	-0.12
	TRAK	-0.53	-0.38	-0.27	-0.25	-0.80	-0.67	-0.01	-0.03	-0.02
	Ours	0.96	0.84	0.72	-0.21	-0.80	-0.67	0.24	0.27	0.19

infeasible for LLMs. Recently, gradient-based methods emerged as efficient alternatives, leveraging model gradients and checkpoints for data valuation. TracIn [50] specifically traces the gradient descent path of training, estimating influence based on gradient similarity across training checkpoints. TRAK [51] approximates the influence using kernel methods derived from gradients and efficient random projections, scaling effectively to large-scale models and datasets. DAVINZ [48] leverages the NTK to estimate data valuation directly from initialization gradients, enabling a training-free evaluation. LOGRA [49] introduces a label-only gradient attribution approach, estimating data valuation by analyzing gradient alignment without relying on explicit labels. Despite these advances, current methods still face significant limitations when dealing with datasets composed of real and synthetic data.

LLM Model Collapse. LLMs trained with increasing amounts of synthetic data have been observed to suffer from model collapse, a phenomenon where model performance degrades over training [11, 21]. One key cause is synthetic data often exhibits reduced diversity and redundancy in knowledge compared to real data, especially when generated from earlier versions of the same model [54, 55]. As synthetic data are reused or recursively generated, the information content becomes increasingly narrow and biased, resulting in amplified errors [56, 57]. These issues motivate a principled understanding of the LLM training behaviors on datasets of real and synthetic mixtures.

Table 2: Relative scores of our method’s NTK and MMD components of selected data contributors under different training sizes. Scores are min-max normalized across contributors within each subsampling size to highlight relative rankings.

Size	Contributor 1		Contributor 2		Contributor 3		Contributor 4		Contributor 5	
	MMD	NTK								
100	0.00	0.00	0.18	0.55	0.00	0.33	0.38	0.96	1.00	1.00
400	0.00	0.00	0.17	0.53	0.03	0.36	0.20	0.74	1.00	1.00
1,000	0.00	0.00	0.15	0.66	0.03	0.54	0.32	0.91	1.00	1.00
4,000	0.00	0.00	0.23	0.65	0.06	0.53	0.29	0.92	1.00	1.00

7 Conclusion

LLMs trained on datasets composed of real and synthetic mixtures exhibit complex scaling behaviors. In this work, we identify a fine-grained three-phase scaling behavior with two breakpoints, reflecting transitions in the model’s ability to acquire head and tail knowledge. We further derive a general LLM generalization bound to reveal key factors that influence the performance of LLMs. Building on this theoretical bound, we develop a practical data valuation method that estimates the contribution of individual data subsets. Empirical results on four diverse tasks show that our method achieves higher correlation with ground-truth than baseline methods, while remaining computationally efficient at LLM-scale tasks.

References

- [1] Alec Radford, Karthik Narasimhan, Tim Salimans, Ilya Sutskever, et al. Improving language understanding by generative pre-training. 2018.
- [2] Xun Liang, Hanyu Wang, Yezhaohui Wang, Shichao Song, Jiawei Yang, Simin Niu, Jie Hu, Dan Liu, Shunyu Yao, Feiyu Xiong, et al. Controllable text generation for large language models: A survey. *arXiv preprint arXiv:2408.12599*, 2024.
- [3] Renze Lou, Kai Zhang, and Wengpeng Yin. Large language model instruction following: A survey of progresses and challenges. *Computational Linguistics*, 50(3):1053–1095, 2024.
- [4] Aske Plaat, Annie Wong, Suzan Verberne, Joost Broekens, Niki van Stein, and Thomas Back. Reasoning with large language models, a survey. *arXiv preprint arXiv:2407.11511*, 2024.
- [5] Tom B. Brown, Benjamin Mann, Nick Ryder, Melanie Subbiah, Jared Kaplan, Prafulla Dhariwal, Arvind Neelakantan, Pranav Shyam, Girish Sastry, Amanda Askell, Sandhini Agarwal, Ariel Herbert-Voss, Gretchen Krueger, Tom Henighan, Rewon Child, Aditya Ramesh, Daniel M. Ziegler, Jeffrey Wu, Clemens Winter, Christopher Hesse, Mark Chen, Eric Sigler, Mateusz Litwin, Scott Gray, Benjamin Chess, Jack Clark, Christopher Berner, Sam McCandlish, Alec Radford, Ilya Sutskever, and Dario Amodei. Language models are few-shot learners. 2020. URL <https://proceedings.neurips.cc/paper/2020/hash/1457c0d6bfcb4967418bfb8ac142f64a-Abstract.html>.
- [6] Jordan Hoffmann, Sebastian Borgeaud, Arthur Mensch, Elena Buchatskaya, Trevor Cai, Eliza Rutherford, Diego de Las Casas, Lisa Anne Hendricks, Johannes Welbl, Aidan Clark, Tom Hennigan, Eric Noland, Katie Millican, George van den Driessche, Bogdan Damoc, Aurelia Guy, Simon Osindero, Karen Simonyan, Erich Elsen, Jack W. Rae, Oriol Vinyals, and Laurent Sifre. Training compute-optimal large language models. *CoRR*, abs/2203.15556, 2022. doi: 10.48550/ARXIV.2203.15556. URL <https://doi.org/10.48550/arXiv.2203.15556>.
- [7] Nandan Thakur, Jianmo Ni, Gustavo Hernández Ábrego, John Wieting, Jimmy Lin, and Daniel Cer. Leveraging llms for synthesizing training data across many languages in multilingual dense retrieval. *arXiv preprint arXiv:2311.05800*, 2023.
- [8] Meishan Zhang, Gongyao Jiang, Shuang Liu, Jing Chen, and Min Zhang. Llm-assisted data augmentation for chinese dialogue-level dependency parsing. *Computational Linguistics*, 50(3):867–891, 2024.
- [9] Jie Chen, Yupeng Zhang, Bingning Wang, Wayne Xin Zhao, Ji-Rong Wen, and Weipeng Chen. Unveiling the flaws: exploring imperfections in synthetic data and mitigation strategies for large language models. *arXiv preprint arXiv:2406.12397*, 2024.
- [10] Mohamed El Amine Seddik, Suei-Wen Chen, Soufiane Hayou, Pierre Youssef, and Merouane Abdelkader DEBBAH. How bad is training on synthetic data? a statistical analysis of language model collapse. In *First Conference on Language Modeling*, 2024. URL <https://openreview.net/forum?id=t3z6U1V09o>.

[11] Ilia Shumailov, Zakhar Shumaylov, Yiren Zhao, Nicolas Papernot, Ross J. Anderson, and Yarin Gal. AI models collapse when trained on recursively generated data. *Nat.*, 631(8022):755–759, 2024. doi: 10.1038/S41586-024-07566-Y. URL <https://doi.org/10.1038/s41586-024-07566-y>.

[12] Yuji Zhang, Sha Li, Jiateng Liu, Pengfei Yu, Yi R Fung, Jing Li, Manling Li, and Heng Ji. Knowledge overshadowing causes amalgamated hallucination in large language models. *arXiv preprint arXiv:2407.08039*, 2024.

[13] Nikhil Kandpal, Haikang Deng, Adam Roberts, Eric Wallace, and Colin Raffel. Large language models struggle to learn long-tail knowledge. In Andreas Krause, Emma Brunskill, Kyunghyun Cho, Barbara Engelhardt, Sivan Sabato, and Jonathan Scarlett, editors, *International Conference on Machine Learning, ICML 2023, 23-29 July 2023, Honolulu, Hawaii, USA*, volume 202 of *Proceedings of Machine Learning Research*, pages 15696–15707. PMLR, 2023. URL <https://proceedings.mlr.press/v202/kandpal23a.html>.

[14] François Charton. Can transformers learn the greatest common divisor? *CoRR*, 2023.

[15] Arthur Jacot, Clément Hongler, and Franck Gabriel. Neural tangent kernel: Convergence and generalization in neural networks. pages 8580–8589, 2018. URL <https://proceedings.neurips.cc/paper/2018/hash/5a4be1fa34e62bb8a6ec6b91d2462f5a-Abstract.html>.

[16] Pang Wei Koh and Percy Liang. Understanding black-box predictions via influence functions. In Doina Precup and Yee Whye Teh, editors, *Proceedings of the 34th International Conference on Machine Learning, ICML 2017, Sydney, NSW, Australia, 6-11 August 2017*, volume 70 of *Proceedings of Machine Learning Research*, pages 1885–1894. PMLR, 2017. URL <http://proceedings.mlr.press/v70/koh17a.html>.

[17] Amirata Ghorbani and James Y. Zou. Data shapley: Equitable valuation of data for machine learning. In Kamalika Chaudhuri and Ruslan Salakhutdinov, editors, *Proceedings of the 36th International Conference on Machine Learning, ICML 2019, 9-15 June 2019, Long Beach, California, USA*, volume 97 of *Proceedings of Machine Learning Research*, pages 2242–2251. PMLR, 2019. URL <http://proceedings.mlr.press/v97/ghorbani19c.html>.

[18] Ruoxi Jia, David Dao, Boxin Wang, Frances Ann Hubis, Nick Hynes, Nezihe Merve Gürel, Bo Li, Ce Zhang, Dawn Song, and Costas J. Spanos. Towards efficient data valuation based on the shapley value. In Kamalika Chaudhuri and Masashi Sugiyama, editors, *The 22nd International Conference on Artificial Intelligence and Statistics, AISTATS 2019, 16-18 April 2019, Naha, Okinawa, Japan*, volume 89 of *Proceedings of Machine Learning Research*, pages 1167–1176. PMLR, 2019. URL <http://proceedings.mlr.press/v89/jia19a.html>.

[19] Jared Kaplan, Sam McCandlish, Tom Henighan, Tom B. Brown, Benjamin Chess, Rewon Child, Scott Gray, Alec Radford, Jeffrey Wu, and Dario Amodei. Scaling laws for neural language models. *CoRR*, abs/2001.08361, 2020. URL <https://arxiv.org/abs/2001.08361>.

[20] Danny Hernandez, Jared Kaplan, Tom Henighan, and Sam McCandlish. Scaling laws for transfer. *CoRR*, abs/2102.01293, 2021. URL <https://arxiv.org/abs/2102.01293>.

[21] Elvis Dohmatob, Yunzhen Feng, Arjun Subramonian, and Julia Kempe. Strong model collapse. *CoRR*, abs/2410.04840, 2024. doi: 10.48550/ARXIV.2410.04840. URL <https://doi.org/10.48550/arXiv.2410.04840>.

[22] Elvis Dohmatob, Yunzhen Feng, Pu Yang, François Charton, and Julia Kempe. A tale of tails: Model collapse as a change of scaling laws. In *Forty-first International Conference on Machine Learning, ICML 2024, Vienna, Austria, July 21-27, 2024*. OpenReview.net, 2024. URL <https://openreview.net/forum?id=KVvku47shW>.

[23] Ayush Jain, Andrea Montanari, and Eren Sasoglu. Scaling laws for learning with real and surrogate data. In *Advances in Neural Information Processing Systems 38: Annual Conference on Neural Information Processing Systems 2024, NeurIPS 2024, Vancouver, BC, Canada, December 10 - 15, 2024*, 2024. URL http://papers.nips.cc/paper_files/paper/2024/hash/c7038ec7eee8dc5a99d74d594f70aa3f-Abstract-Conference.html.

[24] Jaehoon Lee, Lechao Xiao, Samuel Schoenholz, Yasaman Bahri, Roman Novak, Jascha Sohl-Dickstein, and Jeffrey Pennington. Wide neural networks of any depth evolve as linear models under gradient descent. *Advances in neural information processing systems*, 32, 2019.

[25] Greg Yang and Etaf Littwin. Tensor programs iib: Architectural universality of neural tangent kernel training dynamics. In Marina Meila and Tong Zhang, editors, *Proceedings of the 38th International Conference on Machine Learning, ICML 2021, 18-24 July 2021, Virtual Event*, volume 139 of *Proceedings of Machine Learning Research*, pages 11762–11772. PMLR, 2021. URL <http://proceedings.mlr.press/v139/yang21f.html>.

[26] Yuan Cao and Quanquan Gu. Generalization bounds of stochastic gradient descent for wide and deep neural networks. In Hanna M. Wallach, Hugo Larochelle, Alina Beygelzimer, Florence d’Alché-Buc, Emily B.

Fox, and Roman Garnett, editors, *Advances in Neural Information Processing Systems 32: Annual Conference on Neural Information Processing Systems 2019, NeurIPS 2019, December 8-14, 2019, Vancouver, BC, Canada*, pages 10835–10845, 2019. URL <https://proceedings.neurips.cc/paper/2019/hash/cf9dc5e4e194fc21f397b4cac9cc3ae9-Abstract.html>.

[27] Yunzhen Feng, Elvis Dohmatob, Pu Yang, Francois Charton, and Julia Kempe. Beyond model collapse: Scaling up with synthesized data requires verification. *arXiv preprint arXiv:2406.07515*, 2024.

[28] Elvis Dohmatob, Yunzhen Feng, and Julia Kempe. Model collapse demystified: The case of regression. In *Advances in Neural Information Processing Systems 38: Annual Conference on Neural Information Processing Systems 2024, NeurIPS 2024, Vancouver, BC, Canada, December 10 - 15, 2024*, 2024. URL http://papers.nips.cc/paper_files/paper/2024/hash/53dbd7e34fab703a639964e2d3ee9e84-Abstract-Conference.html.

[29] George Kingsley Zipf. *The psycho-biology of language: An introduction to dynamic philology*. Routledge, 2013.

[30] Sanae Lotfi, Marc Finzi, Yilun Kuang, Tim GJ Rudner, Micah Goldblum, and Andrew Gordon Wilson. Non-vacuous generalization bounds for large language models. *arXiv preprint arXiv:2312.17173*, 2023.

[31] Yao Shu, Zhongxiang Dai, Zhaoxuan Wu, and Bryan Kian Hsiang Low. Unifying and boosting gradient-based training-free neural architecture search. *Advances in neural information processing systems*, 35:33001–33015, 2022.

[32] Xiaoqiang Lin, Xinyi Xu, Zhaoxuan Wu, See-Kiong Ng, and Bryan Kian Hsiang Low. Distributionally robust data valuation. In *Forty-first International Conference on Machine Learning, ICML 2024, Vienna, Austria, July 21-27, 2024*. OpenReview.net, 2024. URL <https://openreview.net/forum?id=mbBehLOAqR>.

[33] Mike Fleckenstein, Ali Obaidi, and Nektaria Tryfona. A review of data valuation approaches and building and scoring a data valuation model. *Harvard Data Science Review*, 5(1), 2023.

[34] Jiachen T. Wang and Ruoxi Jia. Data banzhaf: A robust data valuation framework for machine learning. In *International Conference on Artificial Intelligence and Statistics, 25-27 April 2023, Palau de Congressos, Valencia, Spain*, volume 206 of *Proceedings of Machine Learning Research*, pages 6388–6421. PMLR, 2023. URL <https://proceedings.mlr.press/v206/wang23e.html>.

[35] Yongchan Kwon and James Zou. Beta shapley: a unified and noise-reduced data valuation framework for machine learning. In *International Conference on Artificial Intelligence and Statistics, AISTATS 2022, 28-30 March 2022, Virtual Event*, volume 151 of *Proceedings of Machine Learning Research*, pages 8780–8802. PMLR, 2022. URL <https://proceedings.mlr.press/v151/kwon22a.html>.

[36] Xinyi Xu, Zhaoxuan Wu, Chuan Sheng Foo, and Bryan Kian Hsiang Low. Validation free and replication robust volume-based data valuation. In *Advances in Neural Information Processing Systems 34: Annual Conference on Neural Information Processing Systems 2021, NeurIPS 2021, December 6-14, 2021, virtual*, pages 10837–10848, 2021. URL <https://proceedings.neurips.cc/paper/2021/hash/59a3adea76fadcb6dd9e54c96fc155d1-Abstract.html>.

[37] Arthur Gretton, Bharath K. Sriperumbudur, Dino Sejdinovic, Heiko Strathmann, Sivaraman Balakrishnan, Massimiliano Pontil, and Kenji Fukumizu. Optimal kernel choice for large-scale two-sample tests. In Peter L. Bartlett, Fernando C. N. Pereira, Christopher J. C. Burges, Léon Bottou, and Kilian Q. Weinberger, editors, *Advances in Neural Information Processing Systems 25: 26th Annual Conference on Neural Information Processing Systems 2012. Proceedings of a meeting held December 3-6, 2012, Lake Tahoe, Nevada, United States*, pages 1214–1222, 2012. URL <https://proceedings.neurips.cc/paper/2012/hash/dbe272bab69f8e13f14b405e038deb64-Abstract.html>.

[38] Mingsheng Long, Yue Cao, Jianmin Wang, and Michael I. Jordan. Learning transferable features with deep adaptation networks. In Francis R. Bach and David M. Blei, editors, *Proceedings of the 32nd International Conference on Machine Learning, ICML 2015, Lille, France, 6-11 July 2015*, volume 37 of *JMLR Workshop and Conference Proceedings*, pages 97–105. JMLR.org, 2015. URL <http://proceedings.mlr.press/v37/long15.html>.

[39] Dino Sejdinovic, Bharath K. Sriperumbudur, Arthur Gretton, and Kenji Fukumizu. Equivalence of distance-based and rkhs-based statistics in hypothesis testing. *CoRR*, abs/1207.6076, 2012. URL <http://arxiv.org/abs/1207.6076>.

[40] Arthur Gretton, Dino Sejdinovic, Heiko Strathmann, Sivaraman Balakrishnan, Massimiliano Pontil, Kenji Fukumizu, and Bharath K Sriperumbudur. Optimal kernel choice for large-scale two-sample tests. *Advances in neural information processing systems*, 25, 2012.

[41] Alex Krizhevsky, Geoffrey Hinton, et al. Learning multiple layers of features from tiny images. Toronto, ON, Canada, 2009.

[42] Dan Hendrycks and Thomas G. Dietterich. Benchmarking neural network robustness to common corruptions and perturbations. In *7th International Conference on Learning Representations, ICLR 2019, New Orleans, LA, USA, May 6-9, 2019*. OpenReview.net, 2019. URL <https://openreview.net/forum?id=HJz6tiCqYm>.

[43] Andrew L. Maas, Raymond E. Daly, Peter T. Pham, Dan Huang, Andrew Y. Ng, and Christopher Potts. Learning word vectors for sentiment analysis. In Dekang Lin, Yuji Matsumoto, and Rada Mihalcea, editors, *The 49th Annual Meeting of the Association for Computational Linguistics: Human Language Technologies, Proceedings of the Conference, 19-24 June, 2011, Portland, Oregon, USA*, pages 142–150. The Association for Computer Linguistics, 2011. URL <https://aclanthology.org/P11-1015/>.

[44] Hongyang Yang, Xiao-Yang Liu, and Christina Dan Wang. Fingpt: Open-source financial large language models. *FinLLM Symposium at IJCAI 2023*, 2023.

[45] Swaroop Mishra, Daniel Khashabi, Chitta Baral, and Hannaneh Hajishirzi. Natural instructions: Benchmarking generalization to new tasks from natural language instructions. *CoRR*, abs/2104.08773, 2021. URL <https://arxiv.org/abs/2104.08773>.

[46] Zhangchen Xu, Fengqing Jiang, Luyao Niu, Yuntian Deng, Radha Poovendran, Yejin Choi, and Bill Yuchen Lin. Magpie: Alignment data synthesis from scratch by prompting aligned llms with nothing. *CoRR*, abs/2406.08464, 2024. doi: 10.48550/ARXIV.2406.08464. URL <https://doi.org/10.48550/arXiv.2406.08464>.

[47] Jia Li, Edward Beeching, Lewis Tunstall, Ben Lipkin, Roman Soletskyi, Shengyi Huang, Kashif Rasul, Longhui Yu, Albert Q Jiang, Ziju Shen, et al. Numinamath: The largest public dataset in ai4maths with 860k pairs of competition math problems and solutions. *Hugging Face repository*, 13:9, 2024.

[48] Zhaoxuan Wu, Yao Shu, and Bryan Kian Hsiang Low. DAVINZ: data valuation using deep neural networks at initialization. In Kamalika Chaudhuri, Stefanie Jegelka, Le Song, Csaba Szepesvári, Gang Niu, and Sivan Sabato, editors, *International Conference on Machine Learning, ICML 2022, 17-23 July 2022, Baltimore, Maryland, USA*, volume 162 of *Proceedings of Machine Learning Research*, pages 24150–24176. PMLR, 2022. URL <https://proceedings.mlr.press/v162/wu22j.html>.

[49] Sang Keun Choe, Hwijeon Ahn, Juhan Bae, Kewen Zhao, Minsoo Kang, Youngseog Chung, Adithya Pratapa, Willie Neiswanger, Emma Strubell, Teruko Mitamura, Jeff G. Schneider, Eduard H. Hovy, Roger B. Grosse, and Eric P. Xing. What is your data worth to gpt? Ilm-scale data valuation with influence functions. *CoRR*, abs/2405.13954, 2024. doi: 10.48550/ARXIV.2405.13954. URL <https://doi.org/10.48550/arXiv.2405.13954>.

[50] Garima Pruthi, Frederick Liu, Satyen Kale, and Mukund Sundararajan. Estimating training data influence by tracing gradient descent. In Hugo Larochelle, Marc'Aurelio Ranzato, Raia Hadsell, Maria-Florina Balcan, and Hsuan-Tien Lin, editors, *Advances in Neural Information Processing Systems 33: Annual Conference on Neural Information Processing Systems 2020, NeurIPS 2020, December 6-12, 2020, virtual*, 2020. URL <https://proceedings.neurips.cc/paper/2020/hash/e6385d39ec9394f2f3a354d9d2b88eec-Abstract.html>.

[51] Sung Min Park, Kristian Georgiev, Andrew Ilyas, Guillaume Leclerc, and Aleksander Madry. TRAK: attributing model behavior at scale. In Andreas Krause, Emma Brunskill, Kyunghyun Cho, Barbara Engelhardt, Sivan Sabato, and Jonathan Scarlett, editors, *International Conference on Machine Learning, ICML 2023, 23-29 July 2023, Honolulu, Hawaii, USA*, volume 202 of *Proceedings of Machine Learning Research*, pages 27074–27113. PMLR, 2023. URL <https://proceedings.mlr.press/v202/park23c.html>.

[52] Pang Wei Koh, Kai-Siang Ang, Hubert H. K. Teo, and Percy Liang. On the accuracy of influence functions for measuring group effects. In Hanna M. Wallach, Hugo Larochelle, Alina Beygelzimer, Florence d'Alché-Buc, Emily B. Fox, and Roman Garnett, editors, *Advances in Neural Information Processing Systems 32: Annual Conference on Neural Information Processing Systems 2019, NeurIPS 2019, December 8-14, 2019, Vancouver, BC, Canada*, pages 5255–5265, 2019. URL <https://proceedings.neurips.cc/paper/2019/hash/a78482ce76496fcf49085f2190e675b4-Abstract.html>.

[53] Jinsung Yoon, Sercan Ömer Arik, and Tomas Pfister. Data valuation using reinforcement learning. In *Proceedings of the 37th International Conference on Machine Learning, ICML 2020, 13-18 July 2020, Virtual Event*, volume 119 of *Proceedings of Machine Learning Research*, pages 10842–10851. PMLR, 2020. URL [http://proceedings.mlr.press/v119/yoon20a.html](https://proceedings.mlr.press/v119/yoon20a.html).

[54] Alex Havrilla, Andrew Dai, Laura O'Mahony, Koen Oostermeijer, Vera Zisler, Alon Albalak, Fabrizio Milo, Sharath Chandra Raparthy, Kanishk Gandhi, Baber Abbasi, et al. Surveying the effects of quality, diversity, and complexity in synthetic data from large language models. *arXiv preprint arXiv:2412.02980*, 2024.

- [55] Hao Chen, Abdul Waheed, Xiang Li, Yidong Wang, Jindong Wang, Bhiksha Raj, and Marah I Abdin. On the diversity of synthetic data and its impact on training large language models. *arXiv preprint arXiv:2410.15226*, 2024.
- [56] Ilia Shumailov, Zakhar Shumaylov, Yiren Zhao, Yarin Gal, Nicolas Papernot, and Ross Anderson. The curse of recursion: Training on generated data makes models forget. *arXiv preprint arXiv:2305.17493*, 2023.
- [57] Jinghui Zhang, Dandan Qiao, Mochen Yang, and Qiang Wei. Regurgitative training: The value of real data in training large language models. *arXiv preprint arXiv:2407.12835*, 2024.
- [58] Arthur Gretton, Karsten M Borgwardt, Malte J Rasch, Bernhard Schölkopf, and Alexander Smola. A kernel two-sample test. *The Journal of Machine Learning Research*, 13(1):723–773, 2012.
- [59] Shai Ben-David, John Blitzer, Koby Crammer, Alex Kulesza, Fernando Pereira, and Jennifer Wortman Vaughan. A theory of learning from different domains. *Machine learning*, 79:151–175, 2010.
- [60] Richard Socher, Alex Perelygin, Jean Wu, Jason Chuang, Christopher D. Manning, Andrew Y. Ng, and Christopher Potts. Recursive deep models for semantic compositionality over a sentiment treebank. In *Proceedings of the 2013 Conference on Empirical Methods in Natural Language Processing, EMNLP 2013, 18-21 October 2013, Grand Hyatt Seattle, Seattle, Washington, USA, A meeting of SIGDAT, a Special Interest Group of the ACL*, pages 1631–1642. ACL, 2013. URL <https://aclanthology.org/D13-1170/>.
- [61] Jeffrey Zhou, Tianjian Lu, Swaroop Mishra, Siddhartha Brahma, Sujoy Basu, Yi Luan, Denny Zhou, and Le Hou. Instruction-following evaluation for large language models. *CoRR*, abs/2311.07911, 2023. doi: 10.48550/ARXIV.2311.07911. URL <https://doi.org/10.48550/arXiv.2311.07911>.
- [62] Qwen Team. Qwen3, April 2025. URL <https://qwenlm.github.io/blog/qwen3/>.

A Proofs of Theoretical Analysis

This section provides complete proofs for the theoretical analysis. We first give the definition of distribution discrepancy [58] between \mathcal{D}_T and \mathcal{D}_S as a measure to quantify distribution divergence in Definition 1.

Definition 1. *Given any function space \mathcal{H} , the distribution discrepancy between \mathcal{D}_T and \mathcal{D}_S is defined as:*

$$d_{\mathcal{H}}(\mathcal{D}_T, \mathcal{D}_S) \triangleq \sup_{h \in \mathcal{H}} |\mathbb{E}_{\mathbf{x}' \sim \mathcal{D}_T}[h(\mathbf{x}')] - \mathbb{E}_{\mathbf{x} \sim \mathcal{D}_S}[h(\mathbf{x})]|,$$

which can be empirically estimated using samples \mathbf{S} and \mathbf{T} from the respective \mathcal{D}_S and \mathcal{D}_T :

$$d_{\mathcal{H}}(\mathbf{T}, \mathbf{S}) \triangleq \sup_{h \in \mathcal{H}} \left| \frac{1}{|\mathbf{T}|} \sum_{i=1}^{|\mathbf{T}|} h(\mathbf{x}'_i) - \frac{1}{|\mathbf{S}|} \sum_{i=1}^{|\mathbf{S}|} h(\mathbf{x}_i) \right|.$$

We then introduce the following lemma, which is adapted from the proof of Theorem 1 in [48] and the proof of Theorem 2 in [31].

Lemma 2. *Assume that $\lambda_{\min}(\Theta_0) > 0$ and $\|\nabla_{\theta} f(\mathbf{x}; \theta_0)\|_2 \leq B$ for any $(\mathbf{x}, y) \in \mathbf{S}$ sampled from \mathcal{D}_S with $\|\mathbf{x}\|_2 \leq 1$ and $y \in [0, 1]$. Given the loss function $\ell(f, y) \triangleq (f - y)^2/2$ and define $\hat{\mathbf{y}} \triangleq \mathbf{y} - f(\mathbf{x})$, there exist constants $c > 0$ and $M \in \mathbb{N}$ such that for every $m > M$, when applying gradient descent with learning rate*

$$\eta < \min \left\{ 2m^{-1} (\lambda_{\min}(\Theta_{\infty}) + \lambda_{\max}(\Theta_{\infty}))^{-1}, |\mathbf{S}| \lambda_{\max}^{-1}(\Theta_0) \right\},$$

for all the functions f_t obtained during the optimization, with high probability $(1 - \delta)$ over the dataset \mathbf{S} of size $|\mathbf{S}|$, we have

$$\mathcal{L}_{\mathcal{D}_S}(f_t) \leq \mathcal{L}_S(f_t) + 2B \sqrt{\hat{\mathbf{y}}^T \Theta_0^{-1} \hat{\mathbf{y}} / |\mathbf{S}|} + \varepsilon,$$

where $\hat{\mathbf{y}} = [\hat{y}_1, \dots, \hat{y}_{|\mathbf{S}|}]^T$, $\varepsilon \triangleq 2c/\sqrt{m} + 3\sqrt{\log(4/\delta)/2|\mathbf{S}|}$, and $\lambda_{\min}(\cdot), \lambda_{\max}(\cdot)$ denote the minimum and maximum eigenvalue of a matrix, respectively.

With the above definition and lemma, we are now ready to prove Theorem 1.

Theorem 1 (LLM Generalization Bound under Real and Synthetic Mixtures). *Let $\lambda_{\min}(\cdot)$ and $\lambda_{\max}(\cdot)$ denote the minimum and maximum eigenvalue of a matrix. Assume $\lambda_{\min}(\Theta_0) > 0$ and $\|\nabla_{\theta} f(\mathbf{x}; \theta_0)\|_2 \leq B$ for any $(\mathbf{x}, y) \in \mathbf{S}$ with $\|\mathbf{x}\|_2, y \in [0, 1]$. There exist $M \in \mathbb{N}$ such that for every $m > M$, when applying gradient descent with learning rate $\eta < \min \left\{ 2m^{-1} (\lambda_{\min}(\Theta_{\infty}) + \lambda_{\max}(\Theta_{\infty}))^{-1}, |\mathbf{S}| / \lambda_{\max}(\Theta_0) \right\}$, with probability at least $1 - 2\delta$,*

$$\begin{aligned} \mathcal{L}_{\mathcal{D}_T}(f) &\leq \pi \mathcal{L}_{\mathcal{S}_1}(f) + (1 - \pi) \mathcal{L}_{\mathcal{S}_2}(f) + \pi d_{\mathcal{H}}(\mathbf{T}, \mathbf{S}_1) + (1 - \pi) d_{\mathcal{H}}(\mathbf{T}, \mathbf{S}_2) \\ &\quad + 2B \sqrt{\frac{\hat{\mathbf{y}}^T \Theta_0^{-1} \hat{\mathbf{y}}}{|\mathbf{S}|}} + \sqrt{\frac{2 \max(\pi, 1 - \pi) \log(8/\delta)}{|\mathbf{S}|}} + \varepsilon, \end{aligned} \tag{7}$$

where each element in $\hat{\mathbf{y}}$ is defined as $\hat{y} \triangleq y - f(\mathbf{x}; \theta_0)$ and $\varepsilon \triangleq 2c/\sqrt{m} + 3\sqrt{\log(4/\delta)/2|\mathbf{S}|} + \sqrt{\log(4/\delta)/2|\mathbf{T}|} + \mathcal{L}_{\mathcal{D}_T}(f^*) + \mathcal{L}_{\mathcal{D}_S}(f^*)$, and $c > 0$ is a constant.

Proof. Let ϕ_S and ϕ_T be the probability density function for data distribution \mathcal{D}_S and \mathcal{D}_T , respectively. From [59], the generalization performance on \mathcal{D}_T can therefore be bounded using the generalization performance on \mathcal{D}_S by assuming

that the loss function $\ell(\cdot, \cdot)$ is μ -Lipschitz continuous, where $\mu > 0$ denotes a Lipschitz constant:

$$\begin{aligned}
\mathcal{L}_{\mathcal{D}_T}(f) &\leq \mathcal{L}_{\mathcal{D}_T}(f^*) + \mathbb{E}_{(\mathbf{x}, y) \sim \mathcal{D}_T} |\ell(f(\mathbf{x}), y) - \ell(f^*(\mathbf{x}), y)| \\
&\leq \mathcal{L}_{\mathcal{D}_T}(f^*) + \mathbb{E}_{(\mathbf{x}, y) \sim \mathcal{D}_S} |\ell(f(\mathbf{x}), y) - \ell(f^*(\mathbf{x}), y)| + \\
&\quad |\mathbb{E}_{(\mathbf{x}, y) \sim \mathcal{D}_S} |\ell(f(\mathbf{x}), y) - \ell(f^*(\mathbf{x}), y)| - \mathbb{E}_{(\mathbf{x}, y) \sim \mathcal{D}_T} |\ell(f(\mathbf{x}), y) - \ell(f^*(\mathbf{x}), y)|| \\
&\leq \mathcal{L}_{\mathcal{D}_T}(f^*) + \mathbb{E}_{(\mathbf{x}, y) \sim \mathcal{D}_S} [|\ell(f(\mathbf{x}), y) - \ell(f^*(\mathbf{x}), y)|] + \\
&\quad \left| \int (\phi_S(\mathbf{x}) - \phi_T(\mathbf{x})) (\ell(f(\mathbf{x}), y) - \ell(f^*(\mathbf{x}), y)) d\mathbf{x} \right| \\
&\leq \mathcal{L}_{\mathcal{D}_T}(f^*) + \mathbb{E}_{(\mathbf{x}, y) \sim \mathcal{D}_S} (\ell(f(\mathbf{x}), y) + \ell(f^*(\mathbf{x}), y)) + \\
&\quad \mu \left| \int (\phi_S(\mathbf{x}) - \phi_T(\mathbf{x})) |f(\mathbf{x}) - f^*(\mathbf{x})| d\mathbf{x} \right| \\
&\leq \mathcal{L}_{\mathcal{D}_T}(f^*) + \mathbb{E}_{(\mathbf{x}, y) \sim \mathcal{D}_S} \ell(f(\mathbf{x}), y) + \mathbb{E}_{(\mathbf{x}, y) \sim \mathcal{D}_S} \ell(f^*(\mathbf{x}), y) + \\
&\quad \mu \left| \int (\phi_S(\mathbf{x}) - \phi_T(\mathbf{x})) h(\mathbf{x}) d\mathbf{x} \right| \\
&\leq \mathcal{L}_{\mathcal{D}_T}(f^*) + \mathcal{L}_{\mathcal{D}_S}(f^*) + \mathcal{L}_{\mathcal{D}_S}(f) + \mu \sup_{h \in \mathcal{H}} |\mathbb{E}_{\mathcal{D}_S}[h(\mathbf{x})] - \mathbb{E}_{\mathcal{D}_T}[h(\mathbf{x})]| \\
&\leq \mathcal{L}_{\mathcal{D}_T}(f^*) + \mathcal{L}_{\mathcal{D}_S}(f^*) + \mathcal{L}_{\mathcal{D}_S}(f) + \mu d_{\mathcal{H}}(\mathcal{D}_S, \mathcal{D}_T).
\end{aligned} \tag{9}$$

Next, we approximate $d_{\mathcal{H}}(\mathcal{D}_S, \mathcal{D}_T)$ using $d_{\mathcal{H}}(\mathcal{T}, \mathcal{S}_1)$ and $d_{\mathcal{H}}(\mathcal{T}, \mathcal{S}_2)$ where \mathcal{T} , \mathcal{S}_1 , and \mathcal{S}_2 denote the test, real and synthetic datasets. Following Hoeffding's inequality and the assumption stated in the main text that $h(\mathbf{x}) \leq 1$, we have:

$$\begin{aligned}
&\mathbb{P} \left(\left| \mathbb{E}_{\mathcal{D}_S}[h(\mathbf{x})] - \frac{1}{|\mathcal{S}|} \sum_{i=1}^{|\mathcal{S}|} h(\mathbf{x}_i) \right| \geq \varepsilon \right) \\
&\leq \mathbb{P} \left(\left| \mathbb{E}_{\mathcal{D}_S}[h(\mathbf{x})] - \frac{1}{\pi|\mathcal{S}|} \sum_{i=1}^{\pi|\mathcal{S}|} h(\mathbf{x}_i) \right| \geq \frac{\varepsilon}{2\pi} \right) + \\
&\quad \mathbb{P} \left(\left| \mathbb{E}_{\mathcal{D}_S}[h(\mathbf{x})] - \frac{1}{(1-\pi)|\mathcal{S}|} \sum_{i=\pi|\mathcal{S}|+1}^{|\mathcal{S}|} h(\mathbf{x}_i) \right| \geq \frac{\varepsilon}{2(1-\pi)} \right) \\
&\leq 2 \exp \left(-\frac{\varepsilon^2 |\mathcal{S}|}{2\pi} \right) + 2 \exp \left(-\frac{\varepsilon^2 |\mathcal{S}|}{2(1-\pi)} \right) \\
&\leq 4 \max \left\{ \exp \left(-\frac{\varepsilon^2 |\mathcal{S}|}{2\pi} \right), \exp \left(-\frac{\varepsilon^2 |\mathcal{S}|}{2(1-\pi)} \right) \right\} \\
&= 4 \exp \left(-\frac{\varepsilon^2 |\mathcal{S}|}{2 \max(\pi, 1-\pi)} \right).
\end{aligned} \tag{10}$$

Then the following inequality holds with probability at least $1 - \delta$:

$$\begin{aligned}
&|\mathbb{E}_{\mathcal{D}_S}[h(\mathbf{x})] - \mathbb{E}_{\mathcal{D}_T}[h(\mathbf{x})]| - \left| \frac{1}{|\mathcal{S}|} \sum_{i=1}^{|\mathcal{S}|} h(\mathbf{x}_i) - \frac{1}{|\mathcal{T}|} \sum_{i=1}^{|\mathcal{T}|} h(\mathbf{x}'_i) \right| \\
&\leq \left| \mathbb{E}_{\mathcal{D}_S}[h(\mathbf{x})] - \frac{1}{|\mathcal{S}|} \sum_{i=1}^{|\mathcal{S}|} h(\mathbf{x}_i) \right| + \left| \mathbb{E}_{\mathcal{D}_T}[h(\mathbf{x})] - \frac{1}{|\mathcal{T}|} \sum_{i=1}^{|\mathcal{T}|} h(\mathbf{x}'_i) \right| \\
&\leq \sqrt{\frac{2 \max(\pi, 1-\pi) \log(4/\delta)}{|\mathcal{S}|}} + \sqrt{\frac{\log(4/\delta)}{2|\mathcal{T}|}}.
\end{aligned} \tag{11}$$

Based on the inequality above, we can approximate $d_{\mathcal{H}}(\mathcal{D}_S, \mathcal{D}_T)$ using $d_{\mathcal{H}}(\mathbf{T}, \mathbf{S}_1)$ and $d_{\mathcal{H}}(\mathbf{T}, \mathbf{S}_2)$ as below with probability at least $1 - \delta$:

$$\begin{aligned}
d_{\mathcal{H}}(\mathcal{D}_S, \mathcal{D}_T) &= \sup_{h \in \mathcal{H}} |\mathbb{E}_{\mathcal{D}_S}[h(\mathbf{x})] - \mathbb{E}_{\mathcal{D}_T}[h(\mathbf{x})]| \\
&\leq \sup_{h \in \mathcal{H}} \left| \frac{1}{|\mathbf{S}|} \sum_{i=1}^{|\mathbf{S}|} h(\mathbf{x}_i) - \frac{1}{|\mathbf{T}|} \sum_{i=1}^{|\mathbf{T}|} h(\mathbf{x}'_i) \right| + \\
&\quad \sqrt{\frac{2 \max(\pi, 1 - \pi) \log(4/\delta)}{|\mathbf{S}|}} + \sqrt{\frac{\log(4/\delta)}{2|\mathbf{T}|}} \\
&\leq \pi \sup_{h \in \mathcal{H}} \left| \frac{1}{|\mathbf{T}|} \sum_{i=1}^{|\mathbf{T}|} h(\mathbf{x}'_i) - \frac{1}{\pi|\mathbf{S}|} \sum_{i=1}^{\pi|\mathbf{S}|} h(\mathbf{x}_i) \right| + \\
&\quad (1 - \pi) \sup_{h \in \mathcal{H}} \left| \frac{1}{|\mathbf{T}|} \sum_{i=1}^{|\mathbf{T}|} h(\mathbf{x}'_i) - \frac{1}{(1 - \pi)|\mathbf{S}|} \sum_{i=\pi|\mathbf{S}|+1}^{|\mathbf{S}|} h(\mathbf{x}_i) \right| + \\
&\quad \sqrt{\frac{2 \max(\pi, 1 - \pi) \log(4/\delta)}{|\mathbf{S}|}} + \sqrt{\frac{\log(4/\delta)}{2|\mathbf{T}|}} \\
&\leq \pi d_{\mathcal{H}}(\mathbf{T}, \mathbf{S}_1) + (1 - \pi) d_{\mathcal{H}}(\mathbf{T}, \mathbf{S}_2) + \sqrt{\frac{2 \max(\pi, 1 - \pi) \log(4/\delta)}{|\mathbf{S}|}} + \sqrt{\frac{\log(4/\delta)}{2|\mathbf{T}|}}.
\end{aligned} \tag{12}$$

For the empirical loss, we have:

$$\begin{aligned}
L_{\mathbf{S}}(f) &= \frac{1}{|\mathbf{S}|} \sum_{i=1}^{|\mathbf{S}|} \ell(f(\mathbf{x}_i), y_i) \\
&= \frac{\pi}{\pi|\mathbf{S}|} \sum_{i=1}^{\pi|\mathbf{S}|} \ell(f(\mathbf{x}_i), y_i) + \frac{1 - \pi}{(1 - \pi)|\mathbf{S}|} \sum_{i=\pi|\mathbf{S}|+1}^{|\mathbf{S}|} \ell(f(\mathbf{x}_i), y_i) \\
&= \pi L_{\mathbf{S}_1}(f) + (1 - \pi) L_{\mathbf{S}_2}(f).
\end{aligned} \tag{13}$$

Note that $\mu = 1$ for loss function $\ell(f, y) \triangleq (f - y)^2/2$ when $f, y \in [0, 1]$. By combining the results in Eq.(9), Eq.(12) and Eq.(13), and integrating the conclusion in Lemma 2, we complete the proof. \square

Theorem 1 provides a general theoretical understanding of LLMs trained on mixtures of real and synthetic data. Building on this foundation, we next reveal a three-phase transition in the scaling behavior of LLMs under certain assumptions on data and model in Lemma 1.

Lemma 1 (Scaling Behavior with Three phases). *Consider training data where the probability of knowledge i is $q_i = \pi p_i + (1 - \pi)p'_i$, where $p_i \propto i^{-\beta}$ and p'_i is cut off at rank k as defined above. The test error $\mathcal{L}_{\text{test}}$ exhibits distinct scaling regimes characterized by two breakpoints at sample sizes $|\mathbf{S}| = k^\beta$ and $|\mathbf{S}| = k^\beta/\pi$. We have¹:*

Phase 1 (Rapid-Learning): $|\mathbf{S}| \leq c_1 k^\beta$, where c_1 is absolute constant,

$$\mathcal{L}_{\text{test}} \asymp a |\mathbf{S}|^{\frac{1-\alpha-\beta}{\beta}} - b |\mathbf{S}|^{\frac{1-\lambda-\beta}{\beta}} + a k^{1-\alpha-\beta} - b k^{1-\lambda-\beta} + k^{1-\beta}. \tag{5}$$

Phase 2 (Plateau): $c_1 k^\beta < |\mathbf{S}| < c_2 k^\beta/\pi$, where c_2 is absolute constant, $\mathcal{L}_{\text{test}}$ enters a transition state as the limited presence of tail knowledge prevents the rapid learning.

Phase 3 (Tail-Learning): $|\mathbf{S}| \geq c_2 k^\beta/\pi$,

$$\mathcal{L}_{\text{test}} \asymp a(\pi|\mathbf{S}|)^{\frac{1-\alpha-\beta}{\beta}} - b(\pi|\mathbf{S}|)^{\frac{1-\lambda-\beta}{\beta}} + k^{1-\beta}. \tag{6}$$

Proof. From Eq. (9) and triangle inequality, we have

$$\begin{aligned}
\mathcal{L}_{\mathcal{D}_T}(f) &\leq \mathcal{L}_{\mathcal{D}_S}(f) + d_{\mathcal{H}}(\mathcal{D}_S, \mathcal{D}_T) + \mathcal{L}_{\mathcal{D}_T}(f^*) + \mathcal{L}_{\mathcal{D}_S}(f^*) \\
&\leq \mathcal{L}_{\mathcal{D}}(f) + d_{\mathcal{H}}(\mathcal{D}_S, \mathcal{D}) + d_{\mathcal{H}}(\mathcal{D}_S, \mathcal{D}_T) + \mathcal{L}_{\mathcal{D}_T}(f^*) + 2\mathcal{L}_{\mathcal{D}_S}(f^*) + \mathcal{L}_{\mathcal{D}}(f^*) \\
&\leq \mathcal{L}_{\mathcal{D}}(f) + d_{\mathcal{H}}(\mathcal{D}, \mathcal{D}_T) + 2d_{\mathcal{H}}(\mathcal{D}_S, \mathcal{D}) + \mathcal{L}_{\mathcal{D}_T}(f^*) + 2\mathcal{L}_{\mathcal{D}_S}(f^*) + \mathcal{L}_{\mathcal{D}}(f^*),
\end{aligned} \tag{14}$$

¹The notation $g(n) \asymp h(n)$ means that $c_1 h(n) \leq g(n) \leq c_2 h(n)$ for sufficiently large n and absolute constants $c_1, c_2 > 0$.

where \mathcal{D} is the true distribution.

We also have

$$\mathcal{L}_{\mathcal{D}}(f) \leq \mathcal{L}_{\mathcal{D}_T}(f) + d_{\mathcal{H}}(\mathcal{D}_T, \mathcal{D}) + \mathcal{L}_{\mathcal{D}_T}(f^*) + \mathcal{L}_{\mathcal{D}}(f^*). \quad (15)$$

Suppose $d_{\mathcal{H}}(\mathcal{D}, \mathcal{D}_T) = 0$ as \mathcal{D} and \mathcal{D}_T follow the same distribution, then we have

$$\begin{aligned} \mathcal{L}_{\mathcal{D}_T}(f) &= \mathbb{E}_{(\mathbf{x}, y) \sim \mathcal{D}_T} [\ell(f(\mathbf{x}), y)] \\ &\asymp \mathcal{L}_{\mathcal{D}}(f) + d_{\mathcal{H}}(\mathcal{D}_S, \mathcal{D}) = \mathbb{E}_{(\mathbf{x}, y) \sim \mathcal{D}} [\ell(f(\mathbf{x}), y)] + d_{\mathcal{H}}(\mathcal{D}_S, \mathcal{D}) \end{aligned} \quad (16)$$

for any f gained based on the training dataset $\mathbf{S} \sim \mathcal{D}_S$.

Calculating expectation on \mathcal{D}_S , we have:

$$\begin{aligned} E_{\text{test}} &= \mathbb{E}_{\mathcal{D}_S} [\mathbb{E}_{(\mathbf{x}, y) \sim \mathcal{D}_T} [\ell(f(\mathbf{x}), y)]] \\ &\asymp \mathbb{E}_{\mathcal{D}_S} [\mathbb{E}_{(\mathbf{x}, y) \sim \mathcal{D}} [\ell(f(\mathbf{x}), y)]] + \mathbb{E}_{\mathcal{D}_S} [d_{\mathcal{H}}(\mathcal{D}_S, \mathcal{D})]. \end{aligned} \quad (17)$$

For the first term,

$$\begin{aligned} &\mathbb{E}_{\mathcal{D}_S} [\mathbb{E}_{(\mathbf{x}, y) \sim \mathcal{D}} [\ell(f(\mathbf{x}), y)]] \\ &\asymp \sum_{i \geq 1} p_i \left[(1 - (1 - q_i)^{|\mathbf{S}|})(1 - \rho(i)) + (1 - q_i)^{|\mathbf{S}|}(1 - \gamma(i)) \right] \\ &\asymp \sum_{i \geq 1} p_i (1 - \rho(i)) + \sum_{1 \leq i \leq k} p_i (\rho(i) - \gamma(i))(1 - p_i)^{|\mathbf{S}|} + \sum_{i \geq k+1} p_i (\rho(i) - \gamma(i))(1 - \pi p_i)^{|\mathbf{S}|} \\ &\asymp \frac{1}{\beta - 1} - \frac{a}{\alpha + \beta - 1} + \frac{a}{\beta} |\mathbf{S}|^{\frac{1-\alpha-\beta}{\beta}} \left[\Gamma \left(\frac{\alpha + \beta - 1}{\beta}, |\mathbf{S}| k^{-\beta} \right) - \Gamma \left(\frac{\alpha + \beta - 1}{\beta}, |\mathbf{S}| \right) \right] - \\ &\quad \frac{b}{\beta} |\mathbf{S}|^{\frac{1-\lambda-\beta}{\beta}} \left[\Gamma \left(\frac{\lambda + \beta - 1}{\beta}, |\mathbf{S}| k^{-\beta} \right) - \Gamma \left(\frac{\lambda + \beta - 1}{\beta}, |\mathbf{S}| \right) \right] - \\ &\quad \frac{a}{\beta} (\pi |\mathbf{S}|)^{\frac{1-\alpha-\beta}{\beta}} \Gamma \left(\frac{\alpha + \beta - 1}{\beta}, \pi |\mathbf{S}| (k+1)^{-\beta} \right) + \\ &\quad \frac{b}{\beta} (\pi |\mathbf{S}|)^{\frac{1-\lambda-\beta}{\beta}} \Gamma \left(\frac{\lambda + \beta - 1}{\beta}, \pi |\mathbf{S}| (k+1)^{-\beta} \right), \end{aligned} \quad (18)$$

where $\Gamma(s, x) = \int_x^\infty t^{s-1} e^{-t} dt$ is the upper incomplete gamma function.

When $|\mathbf{S}| \leq c_1 k^\beta$, where c_1 is a constant, we have $\Gamma \left(\frac{\alpha + \beta - 1}{\beta}, |\mathbf{S}| k^{-\beta} \right) - \Gamma \left(\frac{\alpha + \beta - 1}{\beta}, |\mathbf{S}| \right) = \Theta(1) - o(1) = \Theta(1)$; when $|\mathbf{S}| > c_1 k^\beta$, we have $\Gamma \left(\frac{\alpha + \beta - 1}{\beta}, |\mathbf{S}| k^{-\beta} \right) - \Gamma \left(\frac{\alpha + \beta - 1}{\beta}, |\mathbf{S}| \right) = o(1) - o(1) = o(1)$. Similarly, when $|\mathbf{S}| \leq c_1 k^\beta$, where c_1 is a constant, we have $\Gamma \left(\frac{\lambda + \beta - 1}{\beta}, |\mathbf{S}| k^{-\beta} \right) - \Gamma \left(\frac{\lambda + \beta - 1}{\beta}, |\mathbf{S}| \right) = \Theta(1) - o(1) = \Theta(1)$; when $|\mathbf{S}| > c_1 k^\beta$, we have $\Gamma \left(\frac{\lambda + \beta - 1}{\beta}, |\mathbf{S}| k^{-\beta} \right) - \Gamma \left(\frac{\lambda + \beta - 1}{\beta}, |\mathbf{S}| \right) = o(1) - o(1) = o(1)$. The test loss for knowledge 1 to k is related to $\sum_{1 \leq i \leq k} p_i \left[(1 - (1 - q_i)^{|\mathbf{S}|})(1 - \rho(i)) + (1 - q_i)^{|\mathbf{S}|}(1 - \gamma(i)) \right]$, thus the breakpoint for head knowledge is $|\mathbf{S}| = c_1 k^\beta$. When $\pi |\mathbf{S}| \geq c_2 k^\beta$, where c_2 is a constant, we have $\Gamma \left(\frac{\alpha + \beta - 1}{\beta}, \pi |\mathbf{S}| (k+1)^{-\beta} \right) = \Theta(1)$; when $\pi |\mathbf{S}| < c_2 k^\beta$, we have $\Gamma \left(\frac{\alpha + \beta - 1}{\beta}, \pi |\mathbf{S}| (k+1)^{-\beta} \right) = \frac{\beta}{1-\alpha-\beta} \Theta((\pi |\mathbf{S}| k^{-\beta})^{\frac{\alpha+\beta-1}{\beta}})$. Similarly, when $\pi |\mathbf{S}| \geq c_2 k^\beta$, where c_2 is a constant, we have $\Gamma \left(\frac{\lambda + \beta - 1}{\beta}, \pi |\mathbf{S}| (k+1)^{-\beta} \right) = \Theta(1)$; when $\pi |\mathbf{S}| < c_2 k^\beta$, we have $\Gamma \left(\frac{\lambda + \beta - 1}{\beta}, \pi |\mathbf{S}| (k+1)^{-\beta} \right) = \frac{\beta}{1-\lambda-\beta} \Theta((\pi |\mathbf{S}| k^{-\beta})^{\frac{\lambda+\beta-1}{\beta}})$. The test loss for knowledge beyond rank k is related to $\sum_{i \geq k+1} p_i \left[(1 - (1 - q_i)^{|\mathbf{S}|})(1 - \rho(i)) + (1 - q_i)^{|\mathbf{S}|}(1 - \gamma(i)) \right]$, thus the breakpoint for tail knowledge is $|\mathbf{S}| = c_2 k^\beta / \pi$.

For the second term,

$$\mathbb{E}_{\mathcal{D}_S} [d_{\mathcal{H}}(\mathcal{D}_S, \mathcal{D})] \asymp \sum_{i=k+1}^{\infty} p_i = \int_{k+1}^{\infty} x^{-\beta} dx = \frac{(k+1)^{1-\beta}}{\beta - 1}. \quad (19)$$

By combining the results above, we complete the proof. \square

B Pseudo Code

This section presents the pseudo code for the proposed data valuation method in Algorithm 1.

Algorithm 1 LLM Data Valuation

1: **Input:** Datasets $\{\mathbf{S}^{(i)}\}_{i=1}^K$ from K contributors, each consists of real and synthetic mixtures; validation set \mathbf{T} ; model f with initialized NTK kernel matrix Θ_0 ; weighting coefficients w_1, w_2, w_3, w_4 .
2: **for** $i = 1$ to K **do**
3: Evaluate $v(\mathbf{S}^{(i)})$ by (8).
4: **end for**
5: **Output:** Valuation scores $\{v(\mathbf{S}^{(i)})\}_{i=1}^K$.

C Generalization to Marginal Evaluation

In LLM-scale training datasets, computing marginal contributions through retraining-based methods like leave-one-out or Shapley value becomes computationally costly due to the model size and dataset scale. To address this, we utilize $v(\mathbf{S})$ as the data valuation function, following the existing work [49, 51].

While this method is our default for LLM-scale applications, our scoring function $v(\mathbf{S})$ remains compatible with marginal estimation for general-purpose data valuation scenarios with smaller models or datasets. Given a collection of data contributors $\{\mathbf{S}^{(1)}, \dots, \mathbf{S}^{(K)}\}$, we define the marginal contribution of contributor i with respect to a coalition $C \subseteq [K] \setminus \{i\}$ as:

$$\Delta_{i,C} = v(\mathbf{S}^C \cup \mathbf{S}^{(i)}) - v(\mathbf{S}^C), \quad (20)$$

where $\mathbf{S}^C = \{\mathbf{S}^{(i)}\}_{i \in C}$. The final value of $\mathbf{S}^{(i)}$ can then be aggregated over all coalitions via:

$$\phi_i = \sum_{C \subseteq [K] \setminus \{i\}} w_C \times \Delta_{i,C}, \quad (21)$$

where $w_C \geq 0$ denotes coalition weights. In particular, for the SV [17], $w_C = |\mathcal{C}|!(K - |\mathcal{C}| - 1)!/K!$. For LOO [16, 52], $w_C = \mathbb{1}_{C \subseteq [K] \setminus \{i\}}$.

D Experiment Details

Here we provide expanded descriptions of the tasks and datasets, baselines, and implementation details that complement Section 5.1.

D.1 Tasks and Datasets

Image Classification. We use the CIFAR-100 dataset [41] as the real data, and generate synthetic data by applying corruption transformations from the CIFAR-100-C benchmark [42]. These transformations include noise (Gaussian, shot, impulse), blur (defocus, glass, motion, zoom), weather (snow, frost, fog, brightness), and digital (contrast, elastic, pixelation, JPEG artifacts). We treat each class as a separate data contributor and use retrained accuracy as the ground-truth for evaluation. We construct the dataset using a long-tail distribution over classes, with the frequency of class i is set as $p_i \propto i^{-2}$. Each data contributor is assigned all the data from a single class, resulting in a total of 100 contributors. The proportion of real data for each contributor is fixed at $\pi = 6.25\%$.

Sentiment Classification. We use the IMDB [43] as the real dataset and the FinGPT Sentiment Train dataset [44] as synthetic data. For evaluation, we use the SST-2 [60] as the test set. Since the test set contains only positive and negative labels, we filter the training data to include only samples with positive and negative labels, excluding neutral samples, to ensure consistency in the binary classification setup. The evaluation metric is accuracy, calculated as the proportion of test samples where the predicted label matches the ground-truth label. We use 10 data contributors, as detailed in Table 3.

Instruction Following. We use the Natural-Instructions dataset [45] as the real dataset and the Magpie-Pro-1M dataset [46] as the synthetic dataset. The test set is the IFEval benchmark [61]. Evaluation is conducted using the IFEval criteria, which include metrics such as instruction-following accuracy—assessing whether the model’s output

Table 3: Data composition of each contributor $S^{(i)}$ in the sentiment classification task. All sample counts are reported in thousands (k), and each contributor contains 14k samples with varying real data proportion π .

Contributor	$S^{(1)}$	$S^{(2)}$	$S^{(3)}$	$S^{(4)}$	$S^{(5)}$	$S^{(6)}$	$S^{(7)}$	$S^{(8)}$	$S^{(9)}$	$S^{(10)}$
Real samples	9	8	7	6	5	4	3	2	1	0
Synthetic samples	5	6	7	8	9	10	11	12	13	14
Total samples	14	14	14	14	14	14	14	14	14	14
π	64%	57%	50%	43%	36%	29%	21%	14%	7%	0%

Table 4: Data composition of each contributor $S^{(i)}$ in the instruction following task. All sample counts are reported in millions (m), and each contributor contains a different total number of samples with a fixed real data proportion π .

Contributor	$S^{(1)}$	$S^{(2)}$	$S^{(3)}$	$S^{(4)}$
Real samples	0.077	0.077	0.077	0.077
Synthetic samples	0.180	0.077	0.033	0.009
Total samples	0.257	0.154	0.110	0.086
π	30%	50%	70%	90%

adheres to the instruction’s intent, format, and constraints, as defined by a set of predefined rules and templates. We use 4 data contributors, as detailed in Table 4.

Complex Reasoning. We use the human-annotated portions of the NuminaMath-CoT training set [47] as real data and the synthetically generated portions as synthetic data. The test set is the NuminaMath-CoT test set. During training, we perform supervised fine-tuning (SFT) by providing complete reasoning steps and final answers to encourage the model to learn CoT reasoning. For evaluation, we employ a powerful language model *Qwen3-32B* [62] as the judgment model to grade the model’s output using in-context learning: given the ground-truth reasoning steps and answer alongside the model’s output, the judgment model determines correctness. The output is deemed correct only if both the reasoning steps and the final answer match the reference solution. For this task, we construct 100 separate data contributors. Specifically, we partition both the real and synthetic datasets into 5050 equal-sized and non-overlapping partitions. Contributor $i \in \{1, \dots, 100\}$ is then assigned $(101 - i)$ partitions of real data and $(i - 1)$ partitions of synthetic data, yielding 100 contributors with varying synthetic-data proportions π .

D.2 Baselines

We compare against four representative baselines designed for efficient data valuation. These baselines are selected based on two criteria: (1) they do not require repeated model retraining, making them scalable to LLMs; and (2) they operate with access to checkpoints, gradients, and training/test data.

- **DAVINZ** [48], which computes data values from NTK-based approximations at initialization.
- **Deviation** [32], which measures deviation in model predictions via kernel ridge regression.
- **LOGRA** [49], a label-only gradient attribution method.
- **TracIn** [50], which tracks training-time gradient similarity.
- **TRAK** [51], which approximates influence scores using randomized kernel projections.

D.3 Implementation Details

All image classification experiments are conducted on a single NVIDIA A100 GPU (80GB). All LLM experiments, including sentiment classification, instruction following, and complex reasoning, are conducted on NVIDIA A100 GPUs (80GB each). To combine the four components in our proposed score (Eq.(8)), we treat their respective weights as tunable hyperparameters. In our paper, we optimize the weights w_1, w_2, w_3, w_4 by fitting a linear regression, where the target is the average of the empirical loss and the MMD score.

E Supplementary Experiments

This section reports additional experimental analysis complementing the main results, including ranking visualization across data valuation methods.

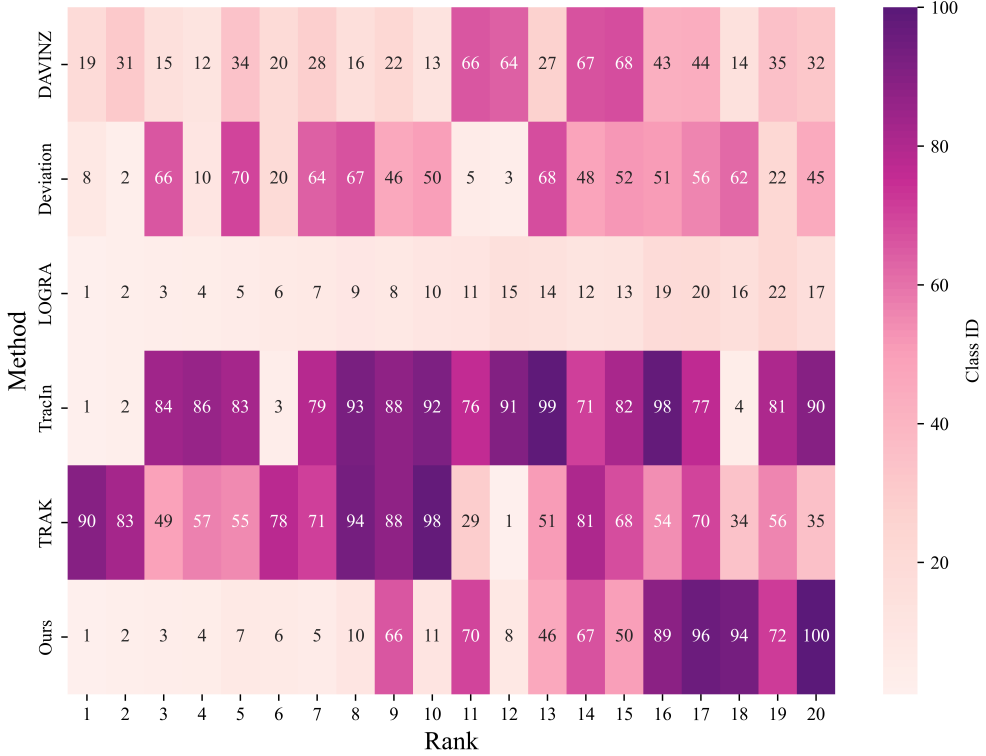


Figure 9: Top-20 contributor selections across data valuation methods on image classification task, where cell colors represent the contributor’s class ID.

To complement correlation-based summaries, we visualize the top-ranked contributors selected by each method on the image classification task. In this task, each contributor corresponds to a single class (100 classes in total), ordered by decreasing sample size (C1 has the most samples while C100 has the fewest). Figure 9 reports the top-20 classes (contributors) deemed most valuable by each data valuation method. We observe that our approach uniquely balances head classes with tail classes, whereas LOGRA, DAVINZ, and Deviation concentrate primarily on head classes, and TracIn and TRAK tend to prioritize tail classes.